Push–Pull Activation of N2: Coordination of Lewis Acids to Dinitrogen Complexes

Anaïs Coffinet, Antoine Simonneau, David Specklin

Push-Pull Activation of N_2: Coordination of Lewis acids to dinitrogen complexes

Anaïs Coffinet, Antoine Simonneau* and David Specklin

LCC-CNRS, Université de Toulouse, CNRS, UPS, 205 route de Narbonne, BP44099, F-31077 Toulouse cedex 4, France.

Abstract: This article gathers, as of 2020, examples of (hetero)dinuclear dinitrogen complexes that are formed by Lewis acid-base interaction thanks to dative bonding between an electron-deficient s-, p- or d-block species and the electron-rich terminal nitrogen of a neutral end-on dinitrogen complex. Lewis acid (LA) coordination to the dinitrogen ligand results in a higher level of activation (i. e. polarization) according to a push-pull mechanism: electron depletion induced by LA coordination amplifies electron back-donation. The magnitude of such phenomenon will depend on various factors that will be highlighted here, as well as the mean to measure it. In some instances, key reactivities that Lewis acid (LA) coordination has lent to the dinitrogen complex, or how their combination has allowed the discovery of original reactions will be discussed. This review is organized in three main sections according to which block of the Periodic System the Lewis acid component of the complexes discussed belongs to. In a final section, pieces of work issued from main group chemistry and relevant in the context of N_2 push-pull activation will be presented.

Keywords: Dinitrogen; transition metal complexes; Lewis acids; Alkali; Alkali-earth; main group; push-pull; heterobimetallic complexes

1. INTRODUCTION

Since the first preparation of an end-on dinitrogen complex in the mid 1960s by Allen and Senoff,[1] N_2 activation has become an important topic in coordination, inorganic and organometallic chemistries. It remains undebatable that transition metal species are predominant in this field. Today, the metals capable of binding dinitrogen span across the whole d-block. A variety of coordination modes are known, albeit the end-on one is frequently encountered.[2–10] Early on, chemists have realized the potential of dinitrogen complexes as platforms to study chemical transformations of the abundant, but very stable and inert N_2 molecule. In relationship with the chemistry occurring in the active site of the nitrogen fixing enzyme nitrogenase,[11–16] one remarkable property of end-on coordinated dinitrogen is its propensity to be protonated by Brønsted acids. Indeed, if sufficient electron density is delocalized into the antibonding π^* molecular orbitals of N_2 by back-donation from the metal, significant basicity is imparted to the terminal nitrogen. In some instances, with excess acid and a sufficiently electron-rich metal, some synthetic dinitrogen complexes have afforded ammonia,[17,18,27–36,19,37–39,20–26] thus mimicking the enigmatic FeMo cofactor necessary for N_2 reduction by the nitrogenases. One great achievement of dinitrogen chemistry is the development of catalytic systems for N_2 reduction by devising sources of protons and electrons that can cohabit long enough within a reactor and that kinetically match NH_3 synthesis over H_2 evolution.[40–46] The remarkably mild reaction conditions under which current homogeneous N_2 reduction catalysts perform are often opposed to the functioning of the industrial Haber-Bosch (HB) process, the only artificial nitrogen fixation technology that has met commercial success and that suffers from high energy and fossil fuel consumptions as well as very harsh operating conditions.[47–53]

Having an estimate of the Brønsted or Lewis basicity of the end-on N_2 ligand is of primary importance for the conception of the above-mentioned catalyses. At the advent of the chemistry of dinitrogen complexes, the preparation and characterization of Lewis acid (LA) adducts of dinitrogen complexes

was therefore envisaged as a valuable source of information, since it would allow one to judge whether the N_2 ligand is accessible to electrophiles in general and what response the transition metal center would give upon complexation of the Lewis acid in terms of $d \rightarrow \pi^*$ electron back donation.[28,54–58] The term "push-pull effect" was soon given to the mechanism by which coordination of a Lewis acid to the terminal nitrogen of an N_2 ligand enhances its "activation",[28,55] a term that has been originally employed for highly polarized olefins featuring electron-withdrawing and -donating groups in a 1,2 relationship.[59,60] Comparatively, the push-pull polarization of N_2 is the result of electron depletion caused by LA complexation (pull effect), resulting in a more important *d* electrons delocalization from the metal (push effect). The same effect has been suggested to be a key factor in biological N_2 activation, operating through H-bond donor sites within the active site of the nitrogenase.[13,61,62] Key analytical probes to measure this effect are typically the N–N bond stretching frequency $\nu(N_2)$ in IR spectroscopy, metrical parameters from X-ray diffraction studies or in some instances, ^{15}N NMR.

The purpose of this article is to gather, as of 2020, examples of *(hetero)dinuclear dinitrogen complexes that are formed by Lewis acid-base interaction thanks to dative bonding between an electron-deficient species and the electron rich terminal nitrogen of a neutral end-on or side-on, end-on dinitrogen complex*. In every case, we will pay attention to place the below-described species within a research context and pick the key available parameters that allow the measurement of the push-pull activation. In some cases, we will discuss key reactivities that Lewis acid (LA) coordination has lent to the dinitrogen complex, or how their combination has allowed the discovery of original reactions. We have decided to organize this review in three main sections according to which block of the Periodic System the Lewis acid component of the complexes discussed belongs to. In a final section, pieces of work issued from main group chemistry and relevant in the context of N_2 push-pull activation will be presented.[63,64]

2. S-BLOCK CATIONS INTERACTION WITH DINITROGEN COMPLEXES

Alkali and alkali-earth cations are used as promoters in a large variety of heterogeneous catalytic processes. Notably, modern catalysts for nitrogen fixation in the Haber-Bosch (H-B) process are incorporating K_2O, CaO and MgO to the iron catalyst bed among other promoters.[53] The calcium and magnesium are limited to a structural role by stabilizing the active sites, increasing the surface area and preserving the integrity of the catalyst. On the other hand, potassium is suspected to have an active participation in the catalysis by acting as an "electronic promoter" on the surface of the catalyst.[49] The effect of such promoters on the catalytic activity has been explored extensively[65] but the results are often empirical and the mechanisms involving the s-group cations are not well understood. This is due in part to the limitations in the investigation of atomic scale interactions on catalysts surfaces, which make extremely difficult the direct observation of the interplay between active sites, substrates and promoters. Understanding the role of these promoters could allow for the development of better-optimized catalysts with effects on their selectivity, activity and robustness.

By comparison, homogeneous systems are more easily studied, allowing for the observation of dynamic processes through direct observation and the isolation of relevant catalytic products and intermediates. The behavior of s-group cations in solution depends on several parameters. Ion pairing can lead to poor solubility, which can be balanced by the use of non-coordinating anions or O- and N-donor solvents that provide weak bonding interactions.[66] Crown ether and cryptands are also able to solvate the cations by host-guest interactions but their coordination often introduce a competition with the substrate.[67] s-Group cations are usually labile, they form interactions lacking significant covalency and are thus mostly electrostatic and non-directional. Despite these limitations, s-group

cations have been found to have an essential role in substrate transformation in molecular catalysis and organic transformations.[68–70]

Fixation and reduction of dinitrogen in the nitrogenase enzyme involve coordination to a reduced iron center embedded in a multimetallic Fe/Fe, Fe/Mo or Fe/V active site. Under an essentially unknown mechanism, sequential reduction and proton transfer reactions occur with low overpotentials and high protonation selectivity.[13] This contrasts with typical iron-based synthetic systems that require metal centers with high π-basicity and high reduction potential, which often results in low selectivity toward protonation.[71,72] A key aspect of biological systems is their use of macroscopic structures to finely control the substrate's environment during enzymatic processes. Secondary-sphere interactions are one of the fundamental tools used by metalloproteins to achieve this control.[73,74] These interactions often involve hydrogen bonding donors and Lewis acidic sites;[75,76] simple s-group cations, especially Na^+ and K^+, are also routinely placed near active sites.[77,78] Insight gained on the nature of bound N_2 ligand / s-group cations interactions could then benefit both homogeneous and heterogeneous N_2 transformation reactions.

2.1. s-Block cations interaction with formally anionic N_2 complexes

Although out of the scope of this review, the association of s-group cations with the N_2 ligand of a formally anionic complex has been observed with a large variety of transition metal (TM) complexes[39,79–81] and deserves some words here. Such interactions are almost exclusively the result of s-block metal promoted reduction of a halide TM complex under an N_2 atmosphere in order to obtain a dinitrogen complex. A 2017 review by Holland and colleagues[82] explored the literature on alkali metal coordination to N_2 complexes, with an emphasis toward insights pertaining to the surface chemistry of the HB process. Typically, coordination of an alkali cation results in a linear M–N≡N–X motif (M: Transition metal, X: alkali cation), the cation being stabilized by coordinating solvent molecules, crown ether solvation or cation-π interactions with the ancillary ligand (Figure 1). By stabilizing electron density on the terminal nitrogen, alkali cation coordination results in activation of the dinitrogen and can promote a nucleophilic reactivity and/or N_2 reduction. At the time of Holland's review, all examples of alkali cations coordination were accompanied with a reduction of the transition metal complex bearing the N_2 ligand and thus the electronic effect of the alkali cations could not be fully resolved. The lack of directly comparable complexes variating the cations also impaired the determination of a clear trend down the alkali group. By comparison, the literature on Alkali-earth cations coordination to dinitrogen is more limited. There is only a handful of studies, which are all restricted to Mg^{2+}. Mirroring most of the alkali cations literature, these examples involve a reduction of the TM complex (directly with Mg^0 or *via* $MgEt_2$ promoted reductive elimination) prior to Mg^{2+} interaction with N_2.[83–87] The coordination of Mg^{2+} generally form a bridging M-N_2-Mg(L_n)-N_2-M motif (M = Mo, Co, Fe; L = THF; n = 2 or 4) with linear or bent N-N-Mg geometries depending respectively on whether the reduction took place at the N_2 ligand to form diazenido (e.g. $[Mo^0\text{-}N{=}N]^{-}$[83–85]) complexes or at the TM center (e.g. $[Co^{-I}\text{-}N{\equiv}N]^{-}$[88]). Owing to reduction events occurring concomitantly with Mg^{2+} coordination, the cation effect on N_2 activation cannot be easily discerned from the inherent properties of the anionic TM species and ion pairing interactions.

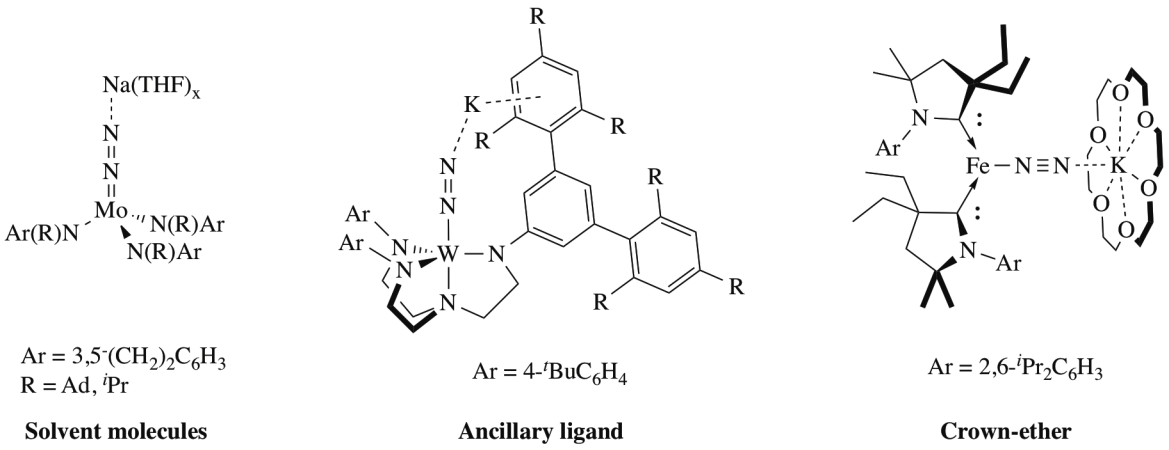

Figure 1. Support of the alkali cations coordination to end-on N_2 ligand.

2.2. Alkali cations interaction with neutral N_2 complexes

In the active site of the nitrogenase enzymes, enhanced N_2 polarization owing to acidic residues (H-bond donors) *via* a "push-pull" mechanism has been proposed to justify the high selectivity and soft conditions required for nitrogen fixation. In this context, the group of Szymczak carried out in 2017 a systematic investigation on the electronic and structural effect of LA coordination to a model iron(0) dinitrogen complex.[61] They reacted $[Fe(depe)_2(N_2)]$ (**1**) (depe: 1,2-bis(diethylphosphino)ethane) with various LAs to afford stable adducts with alkali cations (Scheme 1), Fe^{II} and borane based electrophiles coordinating to the terminal nitrogen of the end-on N_2 ligand. The bulk of their findings concerned the adduct of main group $B(C_6F_5)_3$ that will be discussed in details in section 4.3.1. Complex (**1**) is especially apt for the evaluation of N_2-alkali cations pairing as its neutral state and ligand design allow the pairs to be devoid of charge pairing and cation-π interactions.

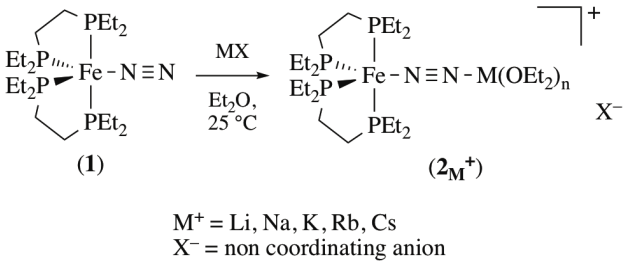

Scheme 1. Formations of adducts ($\mathbf{2_M^+}$) with alkali cations salt of non-coordinating anions $[B(C_6F_5)_4]^-$ or $[B(3,5\text{-}\{CF_3\}_2C_6H_3)_4)]^-$.

The binding of Li^+, Na^+, K^+, Rb^+ and Cs^+ to (**1**) were characterized by IR spectroscopy in Et_2O from freshly prepared stoichiometric mixtures of (**1**) and the salts of non-coordinating anions $Li[B(C_6F_5)_4]$ and $M[B(3,5\text{-}\{CF_3\}_2C_6H_3)_4]$ (M = Na, K, Rb, Cs). The $\nu(N_2)$ of the corresponding adducts ($\mathbf{2_M^+}$) undergoes bathochromic shifts as a function of the LA strength expressed in Acceptor Number (AN).[89] The $\Delta\nu(N_2)$ are ranging from –51.8 to –68.6 cm^{-1} compared to (**1**), indicative of a moderate N_2 activation. Contrary to previous examples of N_2-alkali cations pairs, (**1**) and ($\mathbf{2_M^+}$) are in equilibrium with association constants (in Et_2O) varying from 430(80) to 94(5) M^{-1} down the alkali series. In this simple system, the magnitude of N_2 activation induced by the interaction with alkali cations was following a quasi-linear relationship with the acceptor number of the cations (Figure 2). Dissociation of ($\mathbf{2_M^+}$) was facilitated by the use of a coordinating solvent, which was required to overcome the poor solubilities of the s-group salts.

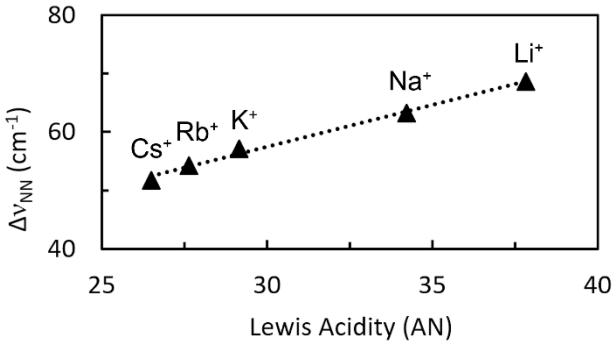

Figure 2. Linear correlation of N_2 stretching frequency and AN for (**2**$_M^+$) (M = Li^+, Na^+, K^+, Rb^+, Cs^+).

In a 2019 study of the alkali series interactions with Molybdenum(0) dinitrogen complexes bearing a family of multidentate lariat ether phosphine ligands, Pap *et al* explored the potential of using tethered crown ethers for alkali cations solvation.[90] Reaction of the triphosphine ligands ({aza-n-crown}CH_2CH_2)$P(CH_2CH_2PPh_2)_2$ (n-crown-P_3-Ph, n = 15, 18) with $MoCl_3(THF)_3$ followed by reduction with Na/Hg in presence of PMe_3 afforded the N_2 complexes **3**^{n}. The related complex *mer*-(n-crown-P_3-^{i}Pr)$Mo(N_2)_2(PPh_2Me)$ (**4**^{n}) was isolated by ligand substitution between $Mo(N_2)_2(PPh_2Me)_4$ and (n-crown-P_3-^{i}Pr). Complexes **3**^{n} and **4**^{n} display tethered crown ethers of different ring sizes in *cis* position to the N_2 ligand, which allowed them to support alkali cations/N_2 interactions (Figure 3).

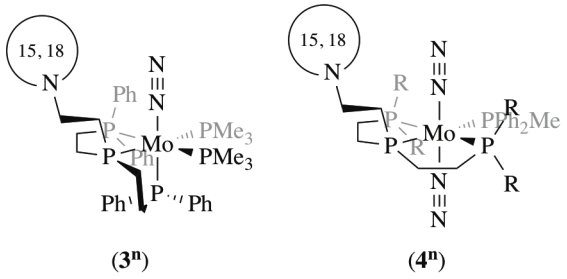

Figure 3. Complexes (**3**^{n}) and (**4**^{n}) bearing tethered *n*-crown ether (R = ^{i}Pr).

Owing to the large cations size disparity within the alkali series, crown ethers of different ring sizes present clear binding selectivities,[91] although the affinity is strong between cations and rings of any size. Salts $M^+[B(C_6F_5)_4]^-$ (M^+ = $[Li(OEt_2)_2]^+$, Na^+, K^+, Rb^+, Cs^+) were reacted with (**3**^{n}) and (**4**^{n}) in *ortho*-difluorobenzene to observe complex behaviors, the respective predominant species (**5**^n_M) and (**6**^n_M) (M = alkali cation) resulted from the sequestration of the cations within the crown ether. The N_2 bound and unbound isomers of these species are in equilibrium (Scheme 2), with relative concentrations depending on the alkali cations. The relative amount of (**5**^n_M) bound isomers grew with increasing cations size, up to Rb^+, then decreased slightly for Cs^+. This behavior is related to the strength and the structural properties of the crown ether interactions. Small cations such as Li^+ interact strongly with crown ethers, which compete effectively with N_2 interactions. Large cations however tend to "pucker" out of the crown ethers plane, leaving them more exposed for further interactions. On account of steric repulsion from the ^{i}Pr groups, complexes (**6**^n_M) exhibited very little interaction of N_2 with Li^+, Na^+ and K^+. Activation of N_2 by the cations interaction is rather weak with a maximum $\Delta\nu(N_2)$ reached for (**5**$^{15}_{Li}$) at –37 cm^{-1} (± 15 cm^{-1}). DFT calculations carried out on (**5**^n_M) and (**6**^n_M) systems suggested that a longer arm between the phosphine ligand and the crown ethers might result in more favorable interactions.

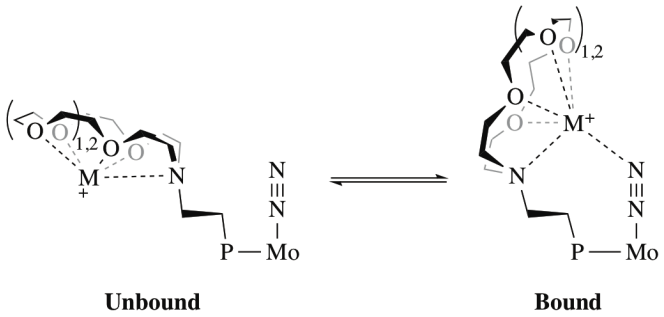

Scheme 2. Equilibrium between bound and unbound isomers of (**5$^{n}_{M}$**) and (**6$^{n}_{M}$**).

Despite a very limited number of examples, interactions of N_2 by alkali cations show an evident correlation between the Lewis acidity of the cations and the degree of N_2 activation. By exploring a simple system presenting no significant competing interactions, Szymczak and his team were able to reveal a linear relationship between the acceptor number of alkali cations and the change in $\nu(N_2)$ stretching frequencies of the interacting N_2 ligand. With no other supporting interactions, coordination of alkali cations to N_2 is weak and labile. Competing interactions such as ions pairing, cation-π interactions and cations solvation can readily overshadow or even prevent the formation of N_2/alkali cations adducts. Taking these considerations into account, careful design of the N_2 complex is needed to profit from alkali cations activation of N_2.

3. LEWIS ACID-BASE ADDUCTS OF END-ON DINITROGEN COMPLEXES WITH D-BLOCK ELECTROPHILES

Early on, after the first few isolations of complexes bearing an end-on N_2 ligand, the first example of two d-block elements coordinating to a single, bridging N_2 ligand was reported by Taube and coll. with the symmetrical *trans*-$[Ru(NH_3)_5\}_2(\mu\text{-}N_2)]^{4+}$.[92] These homobimetallic complexes are typically symmetrical and linear. The resulting lack of N_2 polarization complicate their consideration as mere Lewis pairs, this type of complexes will not be discussed in details, at the exception of two mixed-valence homobimetallic iron complexes presented in section 3.5. Bridged homobimetallic complexes have been reported for a large variety of TMs, encompassing metal centers of group 4 to 10 with end-on, side-on and mixed coordination modes for the N_2 ligand at various activation levels.[2–10]

Weak N_2 activation where the ligand can be formally considered as $(N_2)^0$ occurs more frequently with 18 electrons, mid to late transition metal complexes. Often, the coordination of the second metal center does not influence significantly the N_2 activation and the parameters determining the formation of bridged N_2 complexes over mononuclear complexes are not well understood. The N_2 ligand is typically easily removed under vacuum and chemical activation is seldom encountered.[93] Higher activation of the N_2 ligand (formally $(N_2)^{2-}$ to $(N_2)^{4-}$) occurs more frequently with early TMs with high reducing power to form strong multiple N–Metal bonds. Some of these complexes have been shown to promote the further reduction of N_2 either chemically or electrochemically as well as the reaction of N_2 with small molecules such as H_2[94,95] and CO.[96–100] High activation of N_2 can also lead to splitting by dinuclear complexes to afford nitride complexes as demonstrated by Cummins with $[(Mo\{N^tBu(C_6H_3Me_2\text{-}3,5)\})_3)_2(\mu\text{-}N_2)]$.[101,102]

Comparatively, there has been much less heterobimetallic bridged N_2 complexes reported. The formation of these complexes occurs through several mechanisms that can be separated into two groups: i) reactions involving significant chemical transformations or ii) formation of Lewis pairs. As it does not represent simple Lewis acid-base interactions the former group will not be discussed in this

review; some typical examples are the immediate reduction of the N_2 ligand upon formation of the U^{IV}/Mo^{IV} μ-$(N_2)^{2-}$ complex [{^{t}Bu(3,5-$Me_2C_6H_3$)N}U(μ-N_2)Mo(N^tBuPh)$_3$] from the corresponding U^{III}(THF) and Mo^{III} complexes,[103] the displacement of a chloride ligand by the reaction of [(N(^{t}Bu)(Ar))Mo-N=N]$_2$[Mg(THF)$_2$] with two equivalents of the Nb^{IV} complex [(^{i}Pr)(Ar)N]$_3$NbCl to afford [(^{i}Pr)(Ar)N]$_3$Nb(μ-N_2)Mo[N(^{t}Bu)(Ar)]$_3$[104] or the formal insertion of a W-N_2 moiety into an M-halide bond as disclosed by the team of Hidai[105,106] with the formation of [WX(PMe_2Ph)$_4$(μ-N_2)MCp_2Cl] complexes (M = Ti, Zr, Hf; X = Cl, I).

Formal Lewis pairs are formed by the reaction of a terminal dinitrogen TM complex with TM LAs. This interaction typically results in activation of the N_2 ligand *via* a push-pull mechanism. The formation of such Lewis pairs have been explored since the first reported example by Chatt *et al* in 1969 with the formation of Re^{I}(μ-N_2)Mo^{IV} heterobimetallic complex.[28] The number of Lewis pairs that have been characterized is relatively low and limited to N_2 complexes of Mo^0, Re^{I} and Fe^0 as Lewis bases. As for the Lewis acids, TMs ranging from group 4 up to group 11 elements were employed.

3.1. Early works on $ClRe(N_2)(PMe_2Ph)_4$ adduct with d-block Lewis Acids

The complex *trans*-[$ReCl(N_2)(PMe_2Ph)_4$] (**7**) is part of a series of rhenium(I) dinitrogen complexes that were among the first well-characterized N_2 complexes[107] and Lewis pair formation between (**7**) and d-block LAs has been extensively exemplified. The idea driving this body of work was to prepare and study polynuclear dinitrogen complexes in order to get some insights into the functioning of the nitrogenase enzymes,[108] of which the bimetallic nature was uncovered at the time. Within the series of adducts they were able to characterize, the N_2 ligand is generally weakly activated with $\nu(N_2)$ and d_{NN} in the 1900–2100 cm^{-1} and 1.1–1.2 Å ranges [1922 cm^{-1} and 1.06 Å for (**7**)], respectively.[109]

The Chatt research group pioneered the exploration on the reactivity of Re^{I}-N_2 complexes with the report that (**7**) could react in dichloromethane with THF or Et_2O solvates of $TiCl_3$, $CrCl_3$, $MoCl_3$ and $MoCl_4$.[28] They proposed at the time that the new products formed, characterized by color changes and bathochromic shifts of $\nu(N_2)$, were adducts of the general formula [$Cl(PMe_2Ph)_4Re(\mu\text{-}N_2)MCl_x(S)_y$] (M = Ti^{III} {**8**}, Cr^{III} {**9**}, Mo^{III} {**10**} and Mo^{IV} {**11**}). However, later studies have shown that (**11**) was misidentified and was instead an adduct of a Mo^{V} complex (*vide infra*). The formation of (**11**) was of special interest to them owing to its possible relevance to the nitrogenase enzyme, which also contains a Mo center. To support the proposed nature of (**11**), tentative analogues such as [$Cl(PMe_2Ph)_4Re(\mu\text{-}N_2)MoCl_4(PEtPh_2)$] (**12**) were prepared [$\nu(N_2)$ = 1810 cm^{-1}]. The considerable activation of N_2 in (**11**) [$\Delta\nu(N_2)$ = –127 cm^{-1}] could be further increased with the use of excess $MoCl_4{\cdot}2Et_2O$ [$\Delta\nu(N_2)$ = –242 cm^{-1}]. Attempts to form adducts with other N_2 complexes characterized at the time were inconclusive, they suggested that a certain level of N_2 activation was necessary to provide sufficient Lewis basicity to the terminal nitrogen atom [$\nu(N_2) < \sim$1970 cm^{-1}].

They expanded upon their findings by applying the same synthetic strategy to a large variety of d-block and main group LAs, the latter will be discussed in section 4.[55] They reacted (**7**) with one to two equivalents of groups 2 to 10 and group 12 transition metal halides. Activation of the N_2 ligand was characterized by their stretching frequencies in infrared spectroscopy whose attribution was validated in some cases with comparison to the $^{15}N_2$ analogous complex (Table 1). Although rhenium(I) is a reasonably stable oxidation state, excess $TiCl_4$ and TiF_4 promoted the formation of rhenium(II) complexes, characterized by a $\sim$80 cm^{-1} hypsochromic shift of $\nu(N_2)$. A similar reactivity was also observed previously between [$ReCl(N_2)(dppe)_2$] (dppe: 1,2-bis(diphenylphosphino)ethane) and Ag^{I} or Cu^{II} salts.[54]

Table 1. Spectroscopic properties (cm^{-1}) of *trans*-[ReCl(N_2)(PMe_2Ph)$_4$] adducts with d-block LAs.

Lewis acid	$\nu(^{14}N_2)$	$\nu(^{15}N_2)$	Ratio
Class (1)			
$TiCl_3$[a]			
$[TiCl_3(MeCN)_3]$[a]	1805	1750	1:1
$[TiCl_3(THF)_3]$[a]			
$ZrCl_4$	1790	1747	1:1
$HfCl_4$	1824	1762	1:2[b]
$[VCl_3(MeCN)_3]$	1800	-	1:1
$NbCl_5$	1630	-	1:1[b]
$TaCl_5$	1695	1635	1:1[b]
$[MoCl_4(Et_2O)_2]$	1795	1745	1:1
$[MoCl_4(THF)_2]$	1795	-	1:1
$[MoCl_4(PMePh_2)_2]$	1810	-	1:1
$[MoCl_4(PEtPh_2)_2]$	1810	-	1:1
$[MoCl_4(Et_2O)_2]$[c]	1680	1625	1:2
$[MoCl_4(THF)_2]$[c]	1680	-	1:2
$[WCl_4(PMe_2Ph)_2]$	1730	-	1:1
$[ReOCl_3(PPh_3)_2]$	1842	-	[d]
Class (2)			
$ScCl_2$	1870	-	[d]
$[CrCl_3(THF)_3]$	1890	-	1:1
$[MoCl_3(THF)_3]$	1850	-	[d]
$FeCl_2(THF)_{1.5}$	1860	1795	[d]
$CoCl_2(THF)_{1.5}$	1855	1795	[d]
$[Pt_2Cl_4(PEt_3)_2]$	1890	1825	[d]

Later studies: [a] Adducts of $TiCl_4$ are formed; [b] Ratio established in reference 118; [c] Mo^V species are formed. [d] Unknown ratio.

This comparison across the d-block revealed two classes of LAs, characterized by the magnitude of the $\nu(N_2)$ bathochromic shift. Activation of N_2 is stronger when the LA has vacant *d* orbitals able to receive electronic density *via* π-bonding, such is the case for the early TMs that demonstrate large $\Delta\nu(N_2)$ (< –100 cm^{-1}, down to –292 cm^{-1}). LAs with occupied (such as $Cr^{III}Cl_3$ or $Fe^{II}Cl_2$) or energetically inaccessible *d* orbitals (such as group 13 elements) tend to provide a much smaller $\Delta\nu(N_2)$ (> –70 cm^{-1}, up to –32 cm^{-1}). These results can be rationalized through the push-pull mechanism of N_2 activation: a lesser "pull" of electronic density to the LA will cause a lesser "push" of electronic density from the metal center to the N_2 π-antibonding orbital. Evidently, the N_2 ligand act as a rather hard base with increased activation going up in the periodic table ($HfCl_4$ to $ZrCl_4$: $\nu(N_2)$ = –34 cm^{-1}; $TaCl_5$ to $NbCl_5$: $\nu(N_2)$ = –65 cm^{-1}). Adducts obtained by the addition of $MoCl_4(L)$ (L = Et_2O, THF, phosphines) displayed very little influence of the L ligand. After careful investigation of the Mo adducts, the authors reformulated (**11**), (**12**) and the new Mo adducts as [$(PMe_2Ph)_4ClRe(\mu\text{-}N_2)MoOCl_3L$] species. The formation of adducts with 1:2 (**7**):LA ratio, which they proposed to be of the form [$(PMe_2Ph)_4ClRe(\mu\text{-}N_2)Mo_2OCl_5L$], was accompanied by shifts of the N_2 vibration exceeding 100 cm^{-1}. Despite the lack of definitive characterizations, complicated by the extreme instability of some of these adducts (less than half could be isolated), the presence of the Re–N≡N–M motif was conclusively demonstrated by selective decomposition of the adducts to recover (**7**) and comparative reactions with *trans*-[ReCl(CO)(PMe_2Ph)$_4$].

These findings have then been expanded upon by several groups, with complete characterizations of some of the complexes described and considerable examination of the Re^{I}-N_2/Group 6 adducts.

3.2. *trans*-[ReCl(N_2)(PMe_2Ph)$_4$] adducts of group 6 halides complexes.

Chatt *et al* proceeded in the characterization of the aforementioned [Cl(PMe_2Ph)$_4$Re(μ-N_2)$CrCl_3$(THF)$_2$] (**9**), obtained from the reaction of (**7**) with $CrCl_3(THF)_3$ in dichloromethane.[56] While no solid-state structure could be obtained, the nature of the complex has been confirmed by elemental analysis, decompositions experiments and the magnetic moment corresponding to a chromium(III) (d^3) and rhenium(I) (low-spin d^6) complex. On exposure to air, (**9**) readily convert to a mixture of (**7**) and the Re^{II} complex [ReCl(N_2)(PMe_2Ph)$_4$]$^+$ (**13**). Oxidation to Re^{II} is facilitated by the Re-N_2-Cr bridge providing a path for rapid Re→O electron transfer when dioxygen attacks the chromium atom. The electronic spectrum of the adduct features an intense absorption band at 537 nm which has been considered through the qualitative depiction of the four-center π molecular orbital in Figure 4 (transition metals d_{xz} and nitrogen p_x orbitals, an equivalent set oriented at 90°, are not represented).

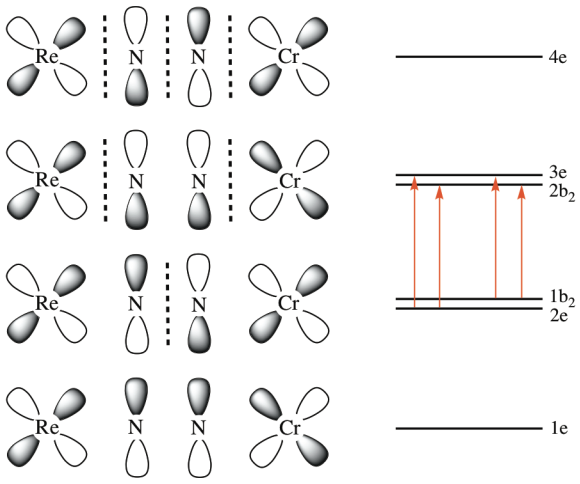

Figure 4. Molecular orbital diagram for **9**. In red: allowed electronic transitions.

The energy of the molecular orbitals (1*e* to 4*e* in idealized C_{4v} symmetry) increases with the number of nodes, with 1*e* and 4*e* orbitals having mainly π(N_2) and π*(N_2) characters, respectively. The intense absorption band can be assigned to a Re→Cr charge transfer as allowed transition occurs from orbitals that are mainly rhenium in character (2*e*: d_{xz}, d_{yz}; 1b_2: δ bonding d_{xy}) to orbitals that are mainly chromium in character (3*e*: d_{xz}, d_{yz}; 2b_2: δ bonding d_{xy}). These orbital considerations are applicable to all Re^{I}-N_2 adducts of TM LAs, that all display significant charge-transfer bands. Moreover, the orbital 2*e* is π*(N_2) in character while 3*e* is π(N_2), 2*e* is completely filled in Re–N≡N–M complexes but the population of 3*e* will depend on the electronic configuration of the LA. This electronic interpretation fits nicely with the separation in two classes of LAs uncovered empirically in previous studies from the group of Chatt: LAs with d^0, d^1 or d^2 configurations lead to a vacant or singly occupied 3*e* orbital which gives rise to a higher N_2 activation than with LAs with higher d electrons count (3*e* doubly occupied and more).

In a series of publications, Mercer and Cradwick tackled on the structural characterizations by X-ray diffraction of adducts formed by the reaction of (**7**) and $MoCl_4(L)_2$ (Figure 5). Reaction of a twofold excess amount of $MoCl_4(THF)_2$ with (**7**) in a CH_2Cl_2/MeOH mixture allowed for the formation over a period of days of the Re^{I}/Mo^{V} adduct [(PMe_2Ph)$_4$ClRe(μ-N_2)$MoCl_4$(OMe)] (**11**).[110,111] The Re-N_2-Mo core is effectively linear, with Re-N (1.82 Å), N-N (1.18 Å) and N-Mo (1.90 Å) distances denoting a significant activation of the N_2 ligand. The N-N distance is elongated but fall short of formal $[N_2]^{2-}$ dimensions

(1.25 Å),[112] the metal nitrogen bonds lengths are intermediate of single and double M-N bonds. This strong N_2 activation is highlighted by a low $\nu(N_2)$ of 1660 cm^{-1}. Two equivalents of (**7**) can react in dichloromethane with $MCl_4(PPh_3)_2$ to yield the trinuclear complexes $[MCl_4\{(\mu\text{-}N_2)ReCl(PMe_2Ph)_4\}_2]$ (M = Mo {**13**}, W {**14**}) by phosphine elimination.[113,114] The solid-state structure of (**13**) could be resolved by X-ray diffraction analysis, showing that (**13**) displays a linear Re-N_2-Mo-N_2-Re motif, analogous to Re^{I}/Ti^{IV} trinuclear complexes discussed hereunder. Dinitrogen activation is lower than in the related dinuclear complex (**11**) as manifested by shorter N-N distances (1.154 Å), longer N-M distances (Re–N = 1.89 Å; Mo–N = 1.98 Å) and higher $\nu(N_2)$ (1800 cm^{-1}). The tungsten analogue (**14**) displays a similar N_2 activation with $\nu(N_2)$ = 1795cm^{-1}.[115]

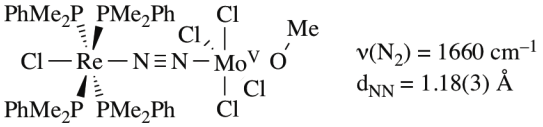

(11)

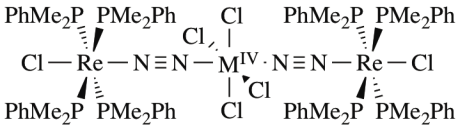

(**13**) (M = Mo) $\nu(N_2)$ = 1800 cm^{-1}; d_{NN} = 1.154 Å
(**14**) (M = W) $\nu(N_2)$ = 1795 cm^{-1}

Figure 5. Structurally characterized Mo and W adducts of Re dinitrogen complexes.

The molybdenum center acts as a ($\delta + \pi$) acceptor, whose properties can be altered by several factors such as oxidation states. The $Mo^{III}Cl_3(THF)_2$ adduct (**10**) displays a relatively high $\nu(N_2)$ value (1858 cm^{-1}) and the $Mo^{V}Cl_4(OMe)$ adduct (**11**) has a much lower $\nu(N_2)$ value (1660 cm^{-1}). Intermediate values are achieved with $Mo^{IV}Cl_4(PR_3)$ (1805–1810 cm^{-1}) or $W^{IV}Cl_4(PMe_2Ph)$ (1740 cm^{-1}). These adducts have essentially the same molecular orbitals bonding schemes than the analogous Cr^{III} adduct (**9**) (Figure 4). Contrary to (**9**) and (**10**), the Mo^{V} d^1 configuration of (**11**) leaves the two 3*e* orbitals vacant, resulting in an elongation of the N–N bond. Because of the singly occupied 3*e* orbitals in the d^2 Mo^{IV} and W^{IV} adducts, intermediate N–N bond lengths are observed.

3.3. *trans*-$[ReCl(N_2)(PMe_2Ph)_4]$ adducts of early TMs halides complexes

The coordination between (**7**) and $TiCl_3$ derivatives were reexamined by Robson.[116] No adducts could be isolated from the reaction of (**7**) and $TiCl_3(THF)_3$ in dichloromethane, however, admission of oxygen into the mixture allowed for the isolation of the $TiCl_4$ derived trinuclear adduct $[TiCl_4\{(\mu\text{-}N_2)ReCl(PMe_2Ph)_4\}_2]\cdot(CH_2Cl_2)_2$ (**15**)$\cdot(CH_2Cl_2)_2$. The color and the $\nu(N_2)$ (1812 cm^{-1}) of (**15**) were virtually identical to adducts reported by Chatt and mistakenly identified as resulting from the coordination of $TiCl_3(L)_2$ (see Table 1). While no solid-state structure could be determined, the Ti^{IV} oxidation state was confirmed by the diamagnetism of the sample. A high yield preparation of (**15**) was achieved by reacting a two-fold excess of (**7**) with $TiCl_4$ in dichloromethane. THF can compete with (**7**) for the coordination to $TiCl_4$, solubilization of (**15**) in THF induced an equilibrium between (**15**) and $[(PMe_2Ph)_4ClRe(\mu\text{-}N_2)TiCl_4(THF)]$ (**16**) [$\nu(N_2)$ = 1755cm^{-1} (THF); 1740 cm^{-1} (Nujol)] (Scheme 3).

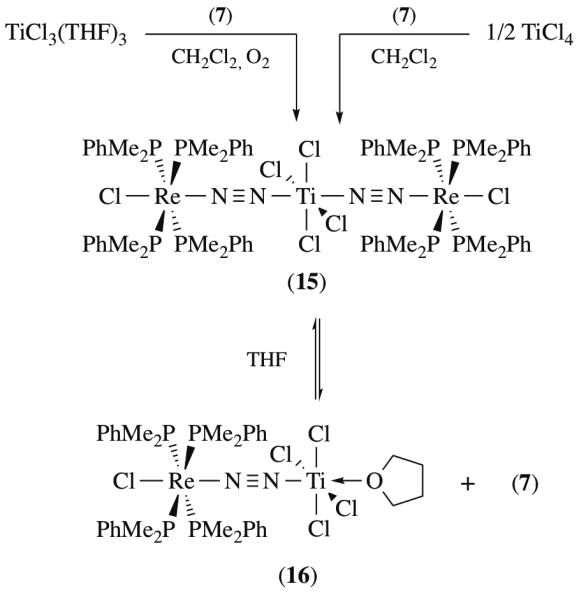

Scheme 3. Formation of (**7**)/$TiCl_4$ adducts.

Contrary to what was observed in Chatt's study, complex (**7**) was found to be resistant to oxidation in the presence of excess $TiCl_4$. Under these conditions, a new adduct with a $\nu(N_2)$ = 1635 cm^{-1} was formed. It remained unidentified but decomposition experiments suggested that it resulted from coordination of two $TiCl_4$. Treatment of this adduct with Et_2O led to the isolation of $[(PMe_2Ph)_4ClRe(\mu\text{-}N_2)(Ti_2Cl_6O)(Et_2O)]$ (**17**) with a $\nu(N_2)$ of 1622 cm^{-1}. It is unclear whether (**17**) is formed by partial hydrolysis of $TiCl_4$ or activation of the C–O bond as such reaction is known to occur between $TiCl_4$ and ethers.[117] Two possibilities have been considered for the structure of (**17**) (not shown): an arrangement with two bridged inequivalent titanium centers in which only one is coordinated to the N_2 ligand or a symmetrical arrangement with two $TiCl_3$ bridged by the terminal nitrogen and oxygen atoms. While the structure has not been categorically identified, the second hypothesis is favored in light of the single type of titanium environment observed by X-ray photoelectron spectroscopy (XPS). In agreement with the electronic considerations discussed above for Re-N_2-M bridges, the coordination to (**7**) of a d^0 metal center induces a strong N_2 activation in (**16**) and (**17**) along with intense charge transfer bands.

In a later study by Donovan-Mtunzi and his team, adducts of (**7**) with group 4 and group 5 halides have been isolated and the N_2 ligand properties characterized by ^{15}N NMR.[118] Adducts $[(PMe_2Ph)_4ClRe(\mu\text{-}N_2)MCl_5]$ (M = Nb {**18**}, Ta {**19**}) have been isolated from equimolar mixtures of (**7**) and the corresponding MCl_5 in dichloromethane. The Zr analogue of (**15**), the trinuclear adduct $[ZrCl_4\{(\mu\text{-}N_2)ReCl(PMe_2Ph)_4\}_2]\cdot C_6H_{14}$ (**20**) has been isolated in the same manner from the hexane solvate of $ZrCl_4$. Owing to the poor solubility of $HfCl_4$ and stability issues, $[HfCl_4\{(\mu\text{-}N_2)ReCl(PMe_2Ph)_4\}_2]$ (**21**) could only be observed in solution within uncharacterized mixtures of compounds. Their $^{15}N_2$ analogues were obtained from $[ClRe(^{15}N_2)(PMe_2Ph)_4]$, the chemical shifts of the $^{15}N_2$ ligand (noted as Re–N_α≡N_β–M) are reported along $\nu(^{14}N_2)$ for adducts (**15**), (**16**) and (**18**)–(**21**) in Table 2.

Table 2. Spectroscopic properties of selected early TMs adducts of (**7**).

Compound	$\nu(N_2)$ cm^{-1}	$\delta(^{15}N_\alpha)$ ppm	$\delta(^{15}N_\beta)$ ppm
$ClRe(N_2)(PMe_2Ph)_4$ (**7**)	1923	–87.2	–63.9
(**7**)-$TiCl_4$(THF) 1:1 (**16**)	1740	–68.1	–19

(**7**)-$NbCl_5$ 1:1 (**18**)	1630	–74.3	–8
(**7**)-$TaCl_5$ 1:1 (**19**)	1695	–76.7	–24.2
(**7**)-$TiCl_4$ 2:1 (**15**)	1812	–76.7	–53.2
(**7**)-$ZrCl_4$ 2:1 (**20**)	1825	–75.9	–95.0
(**7**)-$HfCl_4$ 2:1 (**21**)	1824	–75.4	–96.8

In addition to the clarification of the structures of these already reported complexes,[54] this work addressed the effect of LA coordination to the N_2 ligand on the ^{15}N NMR chemical shifts. In a prior study exploring the ^{15}N NMR of a series of end-on N_2 complexes, the authors observed that the shielding of both nitrogen increased gradually with the atomic number of the transition metal with an expectedly more pronounced effect on N_α than N_β.[119]

In the adducts, both signals are deshielded upon coordination of the LAs and the same periodic dependence is then observed for N_β with shielding increasing along the LA atomic number. There is however little influence of the LA identity on the N_α chemical shift apart from the deshielding caused by the formation of the Lewis pair. From an orbital standpoint, the shielding is related to the splitting of the nitrogen orbitals of the π type. The splitting is larger in ReN_2MN_2Re complex than ReN_2M and the increased shielding from the Ti to the Zr complex reflects the increase in orbital splitting from the first to the second TM series.

3.4. *trans*-[$ReCl(N_2)(PMe_2Ph)_4$] adducts of non-halide TM complexes

In light of previous reports of a diruthenium species bearing a diporphyrin ligand able to oxidize ammonia to form N_2 bridged homometallic complex,[120,121] Zhang *et al*. set out to study the properties of bridged dinitrogen complexes of metalloporphyrins.[122] Because of the *de facto* use of *trans*-[$ReCl(N_2)(PMe_2Ph)_4$] as a model for N_2 complexes coordination to TM LAs, they explored the coordination of (**7**) to iron(III) and chromium(III) porphyrins (Scheme 4). Complexes [Fe(por)(OTf)] (por = octaethylporphyrinate, OEP or tetra(*p*-tolyl)porphyrinate, TTP) react with one equivalent of (**7**) in toluene to afford the bridged heterobimetallic adducts [$(PMe_2Ph)_4ClRe(\mu\text{-}N_2)Fe(por)$][OTf] (por = OEP {**22**}, TTP {**23**}) in moderate yields. Dissociation of the $(OTf)^-$ ligand is necessary to the coordination of N_2 as no reaction is observed with the less labile chloride derivatives. Similarly, (**7**) react with one equivalent of [Cr(OEP)(OTf)] in toluene to yield [$(PMe_2Ph)_4ClRe(\mu\text{-}N_2)Cr(OEP)$][OTf] (**24**).

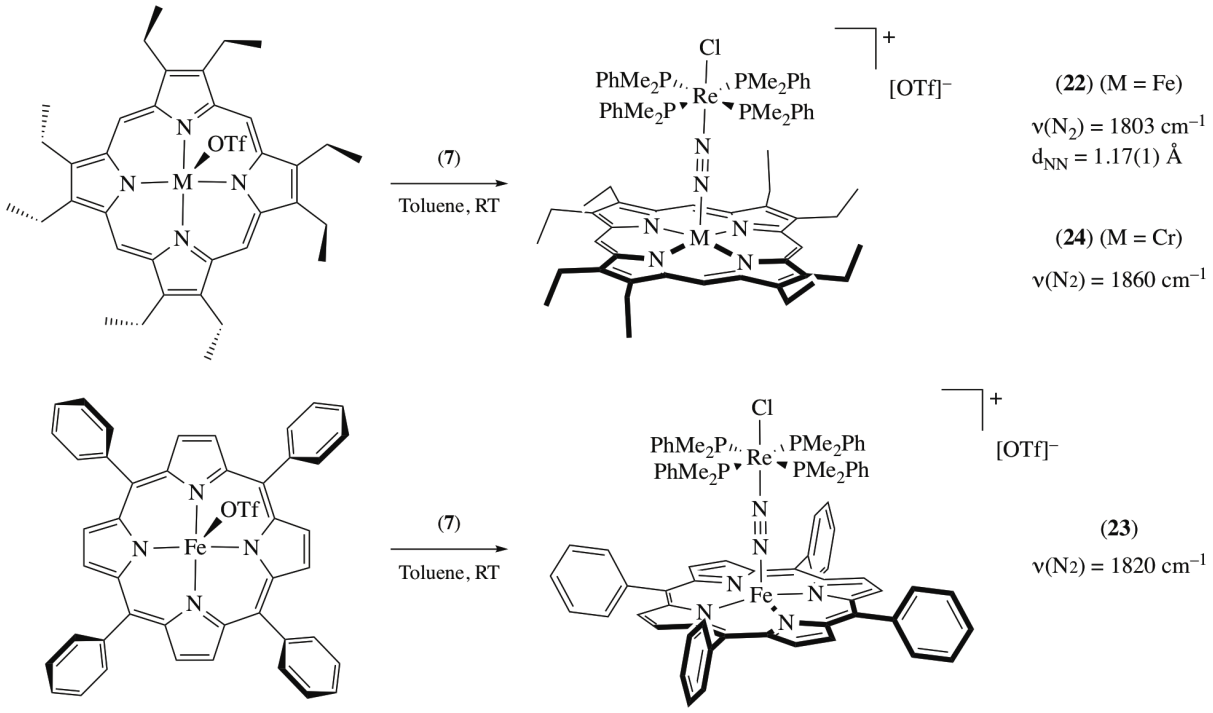

Scheme 4. Formation of bridged N_2 complexes with metalloporphyrins.

The N_2 ligand is moderately activated by the iron complexes with $\nu(N_2)$ = 1803 and 1820 cm^{-1} for (**22**) and (**23**), respectively. These values for d^5 Fe^{III} adducts are expectedly lower than the previously reported d^6 Fe^{II} adduct {$[(PMe_2Ph)_4ClRe(\mu\text{-}N_2)FeCl_2(THF)]$ $\nu(N_2)$ = 1860 cm^{-1}}.[55] The slightly lower N_2 activation by (**23**) is mirrored by a lower formation constant of 240 ± 25 M^{-1} [vs. 410 ± 40 M^{-1} for (**22**)] and is related to the larger steric bulk and lower basicity of TTP compared to OEP. Complex (**24**) displays an even lower formation constant (140 ± 15 M^{-1}) as well as a quite weak N_2 activation [$\nu(N_2)$ = 1887 cm^{-1}], which is comparable to $[Cl(PMe_2Ph)_4Re(\mu\text{-}N_2)CrCl_3(THF)_2]$ [$\nu(N_2)$ = 1860 cm^{-1}].[56] In porphyrin complex (**22**) the iron center display an admixed intermediate spin state (S = $^3/_2$, $^5/_2$) and an upfield pyrrolic resonant signal in ^{1}H NMR, diagnostic of a weakly coordinating weak-field ligand in metalloporphyrins.[123] The solid-state structure of (**22**) exhibits an essentially linear Re-N_2-Fe motif with an elongated N-N distance of 1.17(1) Å. The Re-N distance is longer and the N-N one shorter by *ca.* 0.1 Å than in $[(PMe_2Ph)_4ClRe(\mu\text{-}N_2)MoCl_4(OMe)]$ (**11**), which is coherent with a lower N_2 activation [$\Delta\nu(N_2)$ = +143 cm^{-1} vs (**11**)]. The difference of N_2 activation between the isostructural Fe^{III} and Cr^{III} metalloporphyrins indicates that the relative strength of N_2 acceptors is an interplay of several factors beyond *d* electrons count. Taking into consideration the molecular orbital diagram discussed above (Figure 4), the relatively strong activation for a d^5 LA seen with (**22**) could be related to its intermediate spin state. In the high-spin configuration, two of the *d* orbitals that are occupied are not implicated in the bonding to N_2 and thus the 3*e* orbital, $\pi(N_2)$ in character, is less populated than with low spin d^5 LAs.

The discovery by Cummins of a molybdenum(III) complex able to spontaneously cleave the triple N–N bond of dinitrogen to form metal nitrides has driven an intense curiosity over the possible use of such reactivity in catalytic reduction of N_2.[101] A study of the microscopic reverse of N_2 cleavage, nitride coupling, has been performed by Seymore *et al*. Notably, they observed that the osmium nitride complex $[TpOs(N)Cl_2]$ reacted with the molybdenum nitride complex $[(R_2NCS_2)_3Mo(N)]$ faster than in self-coupling reactions owing to polar effects.[124] In subsequent research, they proposed that such effects could also lower the barrier for N_2 cleavage. To explore this hypothesis, they prepared adducts

of rhenium(I) dinitrogen complexes with the molybdenum(IV) cation $[Mo(S_2CNEt_2)_3]^+$ and assessed whether such adducts could undergo unsymmetrical, "heterolytic" N_2 cleavage (Scheme 5) to form the known molybdenum(VI) $[(Et_2NCS_2)_3Mo(N)]$ and rhenium(V) $[(PMe_2Ph)_4ClReN]^+$ nitrido complexes.[125]

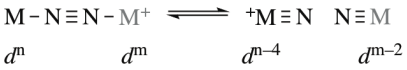

Scheme 5. Unsymmetrical nitride cleavage.

Complex (**7**) reacts in acetone with half an equivalent of $[Mo_2(S_2CNEt_2)_6][OTf]_2$ in three hours to afford the adduct $[(PMe_2Ph)_4ClRe(\mu\text{-}N_2)Mo(S_2CNEt_2)_3][OTf]\cdot Et_2O$ (**25**), isolated in 55 % yield (Scheme 6). The same reaction carried out with *mer*-$[ReCl(N_2)(PMe_2Ph)_2(S_2CNEt_2)]$ results in the adduct $[(S_2CNEt_2)(PMe_2Ph)_2ClRe(\mu\text{-}N_2)Mo(S_2CNEt_2)_3][OTf]$ (**26**), which is stable in solution but decomposes upon isolation. The complex $[ReCl(N_2)(dppe)_2]$ also reacts with $[Mo_2(S_2CNEt_2)_6][OTf]_2$ but the putative adduct $[(dppe)_2ClRe(\mu\text{-}N_2)Mo(S_2CNEt_2)_3][OTf]$ is too unstable to be characterized.

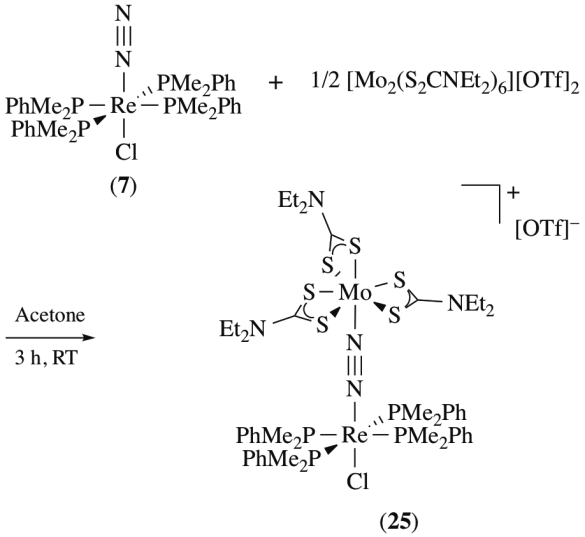

Scheme 6. Synthesis of adduct (**25**).

The lowering of the $\nu(N_2)$ frequencies to 1818 cm^{-1} (**25**) and 1829 cm^{-1} (**26**) induced by coordination of $[Mo(S_2CNEt_2)_3]^+$ is comparable to other examples of dinuclear Re^I/Mo^{IV} bridged complexes (e.g. the series of $MoCl_4(PR_3)$ adducts, see section 3.2). Accordingly, the solid-state structure of (**25**) is very similar to other reported dinuclear adducts (Table 3) with a linear Re-N_2-Mo motif, an elongated N-N distance (1.167 Å) and a shortened Re-N distance (Re-N: 1.858 Å). The Lewis pair nature of (**25**) has been demonstrated by the abstraction of $[Mo(S_2CNEt_2)_3][OTf]$ by PPh_3 to recover (**7**) and $[Mo(PPh_3)(S_2CNEt_2)_3][OTf]$ after 3 h at RT. The instability of (**26**) toward isolation precluded the determination of its solid-state structure but (**26**) is likely to adopt a *mer* geometry according to NMR data.

Table 3. Bond distances of structurally characterized adducts of (**7**).

Compound	Re-N Å	N-N Å	N-M Å
(**7**)	1.87[a]	1.126[a]	-
$[(\mathbf{7})_2MoCl_4]$ (**13**)	1.888	1.154	1.975
$[(\mathbf{7})\text{-}Mo(S_2CNEt_2)_3]^+$ (**25**)	1.858	1.167	1.998
$[(\mathbf{7})\text{-}Fe(OEP)]^+$ (**22**)	1.832	1.17	1.93

[(**7**)-$MoCl_4$(OMe)] (**11**)	1.815	1.18	1.90

[a] Distance approximated according to ref[125]

Heating or photolysis of (**25**) and (**26**) did not result in N_2 cleavage but led to decomposition in mixtures of products. (**7**) and [$ReCl_3(PMe_2Ph)_3$] were identified in minor quantities when (**25**) degraded. Likewise, reduction of (**25**) by electrochemistry or chemical reactants did not induce N_2 cleavage but allowed for the recovery of (**7**). Attempts to react [$(Et_2NCS_2)_3Mo(N)$] and [$ReCl(N)(PMe_2Ph)_4$][OTf] to form (**25**) by nitride coupling were also unsuccessful. These results led to the conclusions that kinetic factors govern the stability of N_2 in this system and the use of polar effects to kinetically favor the cleavage of N_2 will also tend to make it thermodynamically inaccessible.

3.5. Adducts of Mo and Fe N_2 complexes with Fe^{II} Lewis Acids.

There are very few studies of formal TM LAs coordination to dinitrogen complexes of other metallic center than rhenium(I). Unsurprisingly, these examples concern molybdenum and iron centers, whose coordination properties to N_2 have been explored thoroughly owing to their role in nitrogen fixation in both nitrogenase and Haber-Bosch processes.[126,127]

In their seminal work on the chemistry of arene Mo^0 complexes of N_2, Green *et al* were able to isolate a series of Mo^0-N_2 complexes [$(Mo(PR_3)(\eta^6\text{-Ar})(N_2)$] that could also form N_2-bridged dinuclear complexes [$(Mo\{PR_3\}\{\eta^6\text{-Ar}\})_2(\mu\text{-}N_2)$] (Ar = benzene, toluene, mesitylene; PR_3 = PPh_3, $PMePh_2$, PMe_2Ph).[128] While unstable and prone to release the N_2 ligand by reaction with CO or H_2, they remarked that the dinuclear complexes were closely related to the previously isolated N_2-bridged dinuclear complex of Fe^{II} [$(\{Cp\}\{dmpe\}Fe)_2(\mu\text{-}N_2)][BF_4]_2$ (**27**) (dmpe = 1,2-bis(dimethylphosphino)ethane)[129] Given the possible involvement of Mo-N_2-Fe bridged species in the nitrogenase mechanism (which has been later ruled out), they set out to pioneer the characterization of such complexes (Figure 6). Treatment of [Fe(Cp)(dmpe)(Me_2CO)][BF_4] with [Mo(toluene)(N_2)(PPh_3)$_2$] (**28**) was carried out in acetone under argon to afford in 50% yield the Mo^0/Fe^{II} heterobimetallic complex [(toluene)(PPh_3)$_2$Mo(μ-N_2)Fe(Cp)(dmpe)][BF_4] (**29**).

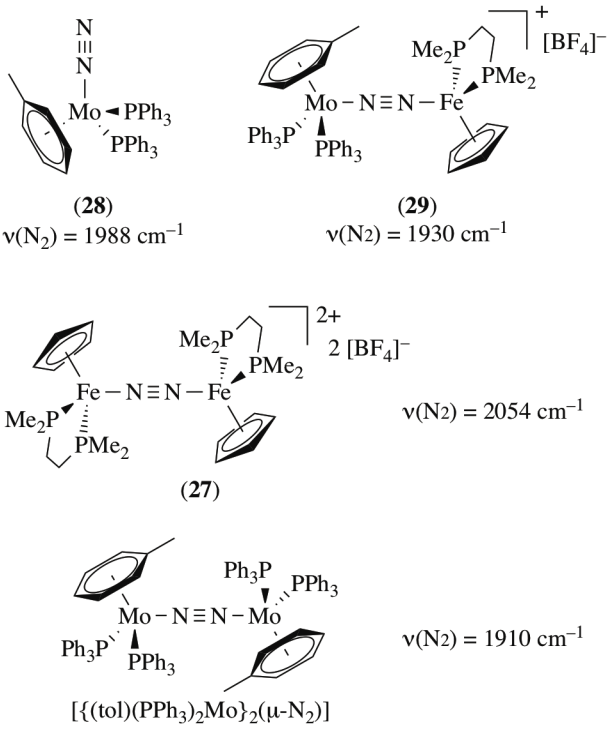

Figure 6. Dinitrogen bridged dinuclear complexes of Mo^0, Fe^{II} and Mo^0/Fe^{II}.

The bridging N_2 is characterized by two bands at 1945 and 1930 cm^{-1} whose relative intensity depend on the solvent used for recrystallisation, acetone-light petroleum ether affording almost exclusively the 1930 cm^{-1} band. The coordination of the Fe^{II} cation resulted in a modest N_2 activation with $\Delta\nu(N_2)$ = –58 cm^{-1} compared to (**28**) (1988 cm^{-1}), which is similar to the effect of $FeCl_2$(THF) coordination to the rhenium(I) complex (**7**) [$\Delta\nu(N_2)$ = –63 cm^{-1}]. The structure of (**29**) is expected to be closely related to the respective homometallic dinuclear adducts of Fe^{II} and Mo^0 with the same ligand system. Due to the symmetry of these dinuclear complexes the bridged N_2 ligand is silent in IR spectroscopy, the Raman vibrations of 1910 cm^{-1} (Mo dimer) and 2054 cm^{-1} (Fe dimer) would infer that the activation level of N_2 ligand in (**29**) is about midway between these homobimetallic complexes.

The group of Schrock has also reported a tetranuclear $FeMo_3$ complex that can formally be depicted as an adduct of an Fe(II) neutral complex with a neutral Mo(III) end-on dinitrogen complex.[83] By the reaction of $\{[N_3N]Mo(N_2)\}_2Mg(THF)_2$ (**30**) ($[N_3N]^{3-}$ = $[(Me_3SiNCH_2CH_2)_3N]^{3-}$) with $FeCl_2$, they were able to isolate a trigonal planar iron complex $\{[N_3N]Mo(N_2)\}_3Fe$ (**31**), formed under a quite unclear mechanism (Figure 7). The solid-state structure reveals that one of the N-N-Fe arrangement is bent, suggesting an iron(II) center stabilized by two anionic $\{[N_3N]Mo(N_2)\}^-$ and one neutral $[N_3N]Mo(N_2)$ ligands. The N_2 ligand embedded in the bent Mo^{III}-N_2-Fe^{II} arrangement shows a comparatively short N-N distance (1.20 Å) against the two other N_2 units (*ca*. 1.26 Å). The lability of one of the Fe–N linkages has been evidenced by treating (**31**) with an excess of THF, leading to equilibrated mixtures of (**31**), $\{[N_3N]Mo(N_2)\}_2Fe(THF)_n$ and $[N_3N]Mo(N_2)$. The latter complex could be prepared separately and analyzed by X-ray diffraction and IR spectroscopy. It is characterized by an N-N distance of 1.09 Å and a $\nu(N_2)$ of 1934 cm^{-1} in pentane. The coordination of the Fe^{II} fragment to this neutral complex, which could not be realized experimentally but formally accomplished in complex (**31**), results in a remarkable bathochromic shift for $\nu(N_2)$ (–231 cm^{-1}) and significant N–N bond elongation (+0.11 Å). Such push-pull activation cannot be accounted for using the model proposed by Chatt and his team (Figure 4) because of the particular geometry of the iron fragment as well as the bent geometry, but trigonal planar $Fe^{II}L_3$ complexes possess a set of 2 vacant antibonding e' orbitals, one of which has the requisite geometry to overlap with a π orbital of the neutral N_2 ligand. Thus, the conditions for strong push-pull activation like those found with d^{0-2} metal complexes (section 3.2) may be met in this case.

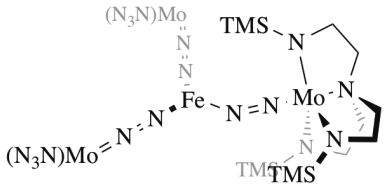

(**31**)

Figure 7. Schrock's tetranuclear $FeMo_3$ dinitrogen complex (**31**) (TMS = trimethylsilyl).

Szymczak and coll. have achieved the synthesis of a mixed-valence Fe^0/Fe^{II} complex showing a bridging dinitrogen between the two metallic centers. As part of their study of the interaction between $[Fe(N_2)(depe)_2]$ (**1**) and various LAs (see sections 2.2 and 4.3.1), they have reacted (**1**) with the sterically accessible high spin d^6 Fe^{II} cation $[Fe(^iPr_2Tp)]^+$ bearing the hydrotris(3,5-iso-propyl-pyrazolyl) borate ligand ($^iPr_2Tp$). The N_2-bridged adduct $[(depe)_2Fe(\mu\text{-}N_2)Fe(^iPr_2Tp)][BAr^F_4]$ [(**32**), Ar^F = 3,5-$(CF_3)_2C_6H_3$] was obtained in excellent yield from the reaction in fluorobenzene of (**1**) with one equivalent of $[FeCl(^iPr_2Tp)]$ in presence of $NaBAr^F_4$ (Scheme 7).[61] Complex (**32**) contains two structurally distinct iron centers and displays a high energy charge transfer band at 910 nm consistent with a mixed-valence complex containing localized Fe^0/Fe^{II} centers. The N_2 ligand is well activated as demonstrated by a lengthening of the N-N distance in the solid-state structure [1.177 Å vs. 1.142 for (**1**)] and the bathochromic shift of the N-N stretching vibration [$\Delta\nu(N_2)$ = –134 cm^{-1}]. This activation is almost

identical than the activation provided by the coordination of $B(C_6F_5)_3$ [$\Delta\nu(N_2) = -129$ cm^{-1}, see section 4.3.1] even though the interaction of these two LAs with N_2 are occurring *via* different orbitals interplay. The orbital situation in (**32**) is comparable to the previously discussed Re^{I}/Cr^{III} adduct and contrasts strongly with the coordination of $B(C_6F_5)_3$ whose interaction between boron's vacant *p* orbital with one of the lobes of the $\pi^*(N_2)$ results in a bent N-N-B geometry (137.0°) and an activation occurring through the lowering of the homo $\pi^*(N_2)$ orbital energy (see section 4.3.1). It is worth mentioning here that the team of Field had previously managed to prepare a cationic dinitrogen-bridged, mixed valence Fe^0/Fe^{II} complex [{(PP_3)FeH}(μ-N_2){Fe(PP_3)}][BPh_4] (**33**) bearing the tetra phosphine ligand $P(CH_2CH_2PMe_2)_3$ (PP_3) (Scheme 7) by selective reduction of an iron(II) hydride center with KO^{t}Bu in the dinuclear end-on bridging dinitrogen Fe^{II}/Fe^{II} complex [(FeH{PP_3})$_2$(μ-N_2)][BPh_4]$_2$ (**34**) (not shown).[130] By contrast with the Fe^0/Fe^{II} complex (**32**) prepared by the Szymczak group, structural data point to the absence of further N_2 activation by the reduction of the Fe^{II} center in (**34**): the linear Fe-N_2-Fe motif displays an N-N distance of 1.127 Å, almost identical to the parent complex (1.129 Å) or the related Fe^0 homobimetallic complex [(Fe{dmpe})$_2$(μ-N_2)] (1.144 Å).[131] The different level of activation provided by the coordination of an Fe^{II} center to a Fe^0-N_2 complex between (**32**) and (**33**) appears to be the result of two parameters. Contrary to (**32**), **33** displays two nearly identical coordination spheres which will diminish any structurally related polarization of the central N_2 ligand. The difference in ligand field strength results in a low spin Fe^{II} center in (**33**) and a high spin Fe^{II} center in (**32**), considering that the dx^2-y^2 and the dz^2 are not taking part in the M-N_2 interaction, a high spin system in d^6 transition metal will result in a less populated *3e* MO (see Figure 4), which is $\pi(N_2)$ in character.

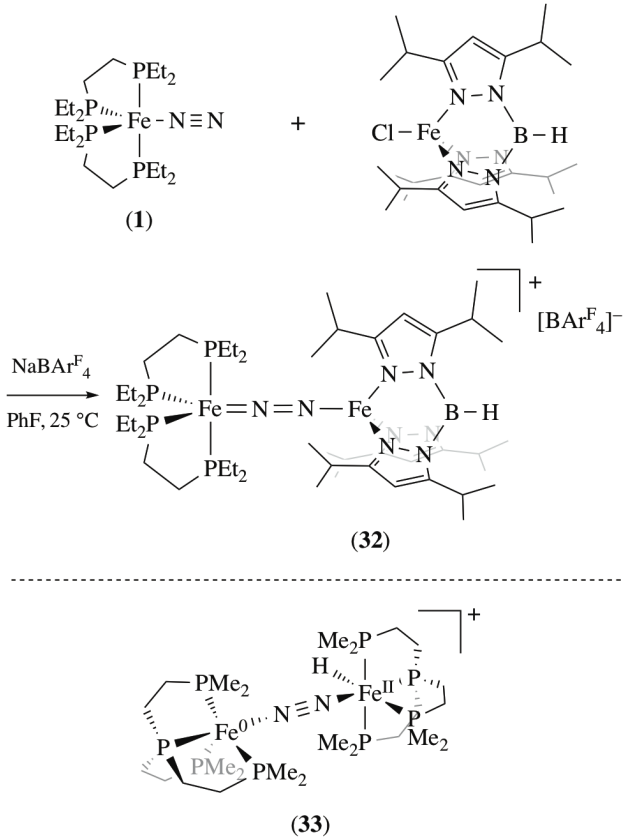

Scheme 7. Formation of complex (**32**) and the mixed-valence Fe^0/Fe^{II} complex (**33**).

4. LEWIS ACID-BASE ADDUCTS OF END-ON DINITROGEN COMPLEXES WITH P-BLOCK ELECTROPHILES

4.1. Adducts with alkyl-aluminum Lewis acids – assessing the basicity of coordinated N_2

As mentioned above, J. Chatt and his group at the Nitrogen Fixation Unit of the University of Sussex systematically investigated the interaction of some end-on dinitrogen complexes with electrophilic transition metal or main-group compounds during the late 60s and the early 70s (see section 3.1). As far as the latter is concerned, the reaction of the Re(I) complex (**7**) with strong electron acceptors such as BCl_3, $AlCl_3$ or $GaCl_3$ led to N_2 evolution. They could however characterize two adducts (**35**) and (**36**) when $AlEt_3$ or PF_5 were employed, respectively, although the compound formed with the latter was thermally unstable (Scheme 8).[55] In the PF_5 adduct, the lowering of the $\nu(N_2)$ stretching frequency observed by infrared (IR) spectroscopy was remarkable [$\Delta\nu(N_2)$ = –283 cm^{-1}]. This was attributed to the delocalization of bonding π-electrons from the N_2 ligand into the phosphorus vacant *d* orbitals. On the contrary, adduct formation with $AlEt_3$ had a weaker effect on $\nu(N_2)$ [$\Delta\nu(N_2)$ = –33 cm^{-1}] since aluminum has no energetically accessible *d* orbitals.

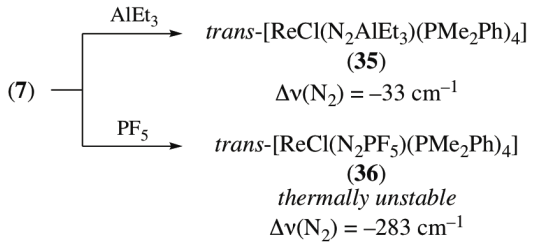

Scheme 8. Adducts of *trans*-[$ReCl(N_2)(PMe_2Ph)_4$] with p-block elements.

In a following article, the same team explored deeper the interaction of trimethylaluminum with various isoelectronic Re^{I}, Mo^{0}, W^{0} and Os^{II} phosphine dinitrogen complexes. The weakening of the N≡N bond observed by IR spectroscopy upon adduct formation suggested, by analogy with what was observed in the case of (**35**), that the trimethylaluminum was bound to the terminal nitrogen. The bis-dinitrogen complexes *trans*-[$M(N_2)_2(dppe)_2$] [dppe = 1,2-bis(diphenylphosphino)ethane, M = Mo or W] (**37**) gave solely 1:1 adducts (**38**) even in the presence of a 30-fold molar excess of trimethylaluminum (Scheme 9), since no band attributable to a 2:1 adduct could be observed in IR spectroscopy. Both complexes (**38**) were characterized by a band assigned to the stretching of the non-bridging dinitrogen ligand and shifted to higher wavenumbers [$\Delta\nu(N_2)$ = +78 cm^{-1} (M = Mo), $\Delta\nu(N_2)$ = +44 cm^{-1} (M = W)], and another one corresponding to the bridging dinitrogen that moved to lower wavenumbers [$\Delta\nu(N_2)$ = –94 cm^{-1} (M = Mo), $\Delta\nu(N_2)$ = –79 cm^{-1} (M = W)]. Some reactivity tests on these adducts were performed: addition of THF or EtOH allowed for the recovery of the starting dinitrogen complexes, with methane evolution in the latter case, while addition of Et_2O led to equilibrated mixtures. Determination of the equilibrium constants K for various dinitrogen complexes by relating the concentration of the different species to their integrated peak heights in the ^1H NMR spectra of equilibrated benzene solutions enabled measurement of the relative basicity of the terminal nitrogen. Higher K related to more basic terminal nitrogen, leading to the following basicity scale: THF > *trans*-[$ReCl(N_2)(PMe_2Ph)_4$] (**7**) > *trans*-[$Mo(N_2)_2(dppe)_2$] (**37_{Mo}**) > *trans*-[$W(N_2)_2(dppe)_2$] (**37_{W}**) > *trans*-[$ReCl(N_2)(PMe_2Ph)_2\{P(OMe)_3\}$] > Et_2O > *mer*-[$OsCl_2(N_2)(PEt_2Ph)_3$]. No correlations between the basic strength with either the ^1H NMR or $\nu(N_2)$ shifts of the adduct were found.

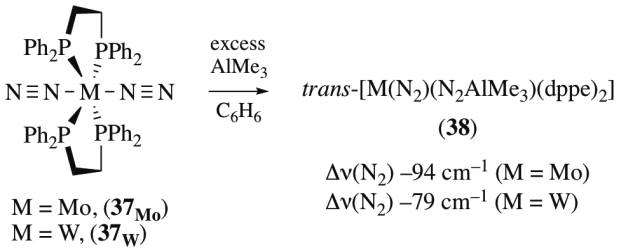

Scheme 9. Adducts of bis-dinitrogen group 6 complexes with $AlMe_3$.

More recently, the team of Tuczek have studied the reaction of trimethylaluminum with a molybdenum complex supported by a tripodal $MeSi(CH_2PMe_2)_3$ (SiP_3) ligand and dppm (dppm = bis(diphenylphosphino)methane).[132] The naked complex $[Mo(N_2)(SiP_3)(dppm)]$ (**39**) exhibited a decent level of N_2 activation as judged by IR spectroscopy [$\nu(N_2)$ = 1952 cm^{-1} in the solid or 1988 cm^{-1} in benzene], but unfruitful reactions with strong Brønsted acids have led them to consider Lewis acid coordination as a mean to assess basicity of the terminal nitrogen atom. The $AlMe_3$ adduct (**40**) was characterized by solution IR spectroscopy [$\Delta\nu(N_2)$ = –107 cm^{-1}] and by ^{31}P NMR: the spectrum showed an upfield resonance for the PMe_2 group in *trans* position to N_2 [shifted from δ –0.4 ppm for the parent complex **39** to δ –12.1 ppm for the LA adduct (**40**)]. The equatorial phosphines were only slightly affected by the adduct formation [$\Delta\delta(PPh_2)$ = –0.3 ppm and $\Delta\delta(PMe_3)$ = –1.4 ppm].

4.2. Adducts of group 6 end-on dinitrogen complexes with fluorinated aryl boranes: N_2 functionalization inspired by the Frustrated Lewis Pair chemistry

In 2017, the team of Simonneau reported the formation of 1:1 adducts between group 6 N_2 complexes $[M(N_2)_2(dppe)_2]$ (**37**) [dppe = 1,2-bis(diphenylphosphino)ethane] and $B(C_6F_5)_3$ (**41**). This study was conducted to assess the push-pull effect using a highly electrophilic borane as LA, in the context of the frustrated Lewis pairs (FLPs) chemistry, but also to devise original reactivities for these metal/main group combinations that activate N_2.

The now mature field of FLPs chemistry exploits the simultaneous action of a LA and a Lewis base (LB), prevented from forming a classical LA–LB adduct by steric interactions, for the activation of a vast array of molecules.[133–136] In a seminal paper by Stephan and coworkers, H_2 could be heterolytically and reversibly cleaved by a simple phosphine-borane,[137] paving the way for the development of metal-free hydrogenation reactions.[138–142] Interestingly, related FLP systems were reported to activate carbon monoxide (CO), which is isoelectronic to N_2. The Erker research group reported that phosphine borane (**42**) reacts with CO[143] to form a five-membered heterocyclic carbonyl compound (**43**) as the result of the following orbital interactions: the non-bonding 3σ orbital localized on carbon mixes with the vacant *p* orbital of the boron atom, while the non-bonding doublet on the phosphorus atom combines with the antibonding π^* of the diatomic molecule, largely developed on the C atom (Scheme 10).

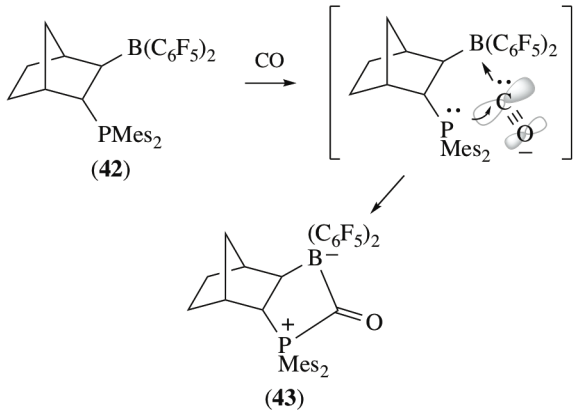

Scheme 10. Activation of CO by an FLP.

The team of Simonneau has been able to quantitatively prepare adducts (**44**) in solution in aromatic solvents (Scheme 11).[144] Their formation was ascertained by several NMR spectroscopy indicators: loss of symmetry in the ^{1}H NMR spectrum, downfield shift of the ^{31}P resonance, upfield shift of the *meta* fluorine signals of (**41**) in ^{19}F NMR and sharpening of the ^{11}B signal and its displacement towards negative chemical shifts, which were strong indicators of boron pyramidalization. The X-ray structures of (**44**) have the following particular features:

i) one of the N_2 ligand in the starting complexes (**37**) has been lost upon coordination of the strong Lewis acid (**41**), leaving one apical site vacant for an agostic interaction between the metal center and an *ortho* hydrogen of one of the phenyl group of the ligand to take place;

ii) the N–N bond is significantly elongated (*ca*. +0.1 Å) compared to the starting complex in which activation of N_2 is weak. This is also corroborated by bathochromic shifts of the $\nu(N_2)$ stretching frequency ($\Delta\nu(N_2)$ *ca*. 230 cm^{-1}) in IR spectroscopy;

iii) the NNB arrangement is bent (*ca*. 140 °).

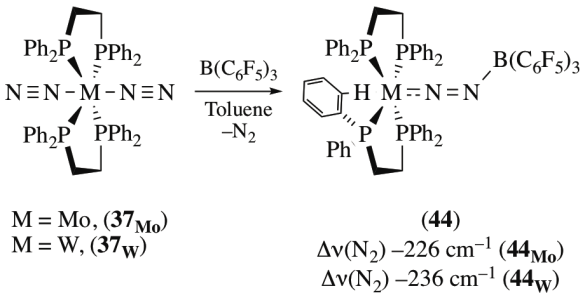

Scheme 11. Adducts of Mo- and W-N_2 complexes with $B(C_6F_5)_3$.

The push-pull activation of N_2 in these systems can be paralleled to the FLP chemistry since the electron-rich transition metal center injects more electron density from its filled *d* orbitals into the antibonding ones of N_2 upon coordination of the borane. However, unlike the "conventional" FLPs that activate CO, adduct formation does not occur through interaction of the lone pair on the terminal nitrogen between the vacancy at boron. Instead, the boron *p* orbital mixes with a π^* orbital of N_2, accounting for the observed bent N-N-B arrangement observed in the solid-state structure. Such orbital mixing was confirmed by theoretical calculations on related complexes of iron(0) (*vide infra*).

The same team demonstrated that their dinitrogen complexes/borane combinations were reactive towards Et_3SiH and $HB(C_6F_5)_2$, resulting in the functionalization of the terminal N with the triethylsilyl

(**45**) and bis(pentaflurorophenyl)boryl (**46**) groups, respectively (Scheme 12). The mechanisms of these transformations were proposed on the basis of already existing data on Si–H[145–147] and B–H[144] bond activation with FLP systems and implies prior dissociation of Lewis pairs (**44**).

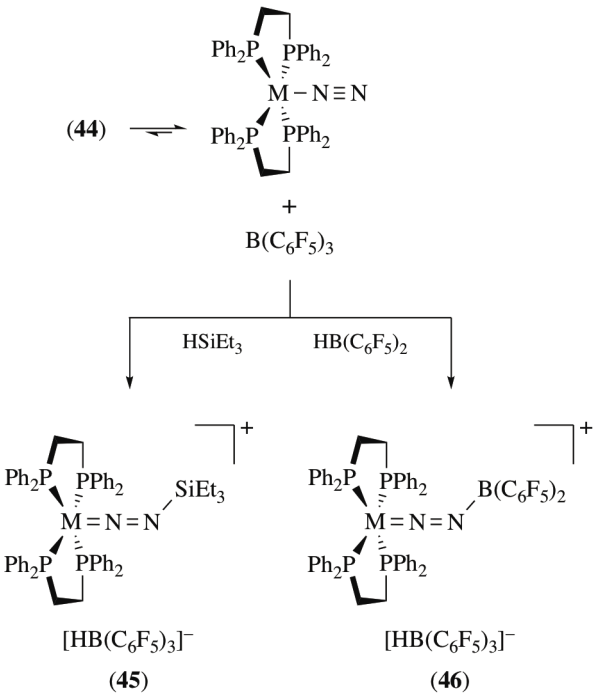

Scheme 12. Functionalization of N_2 based on the FLP-type splitting of B–H and a Si–H bonds.

As a continuation of this work, the team of Simonneau has explored the ability of $HB(C_6F_5)_2$ (**47**), which is a strong Lewis acid as well as a good hydride donor,[148] to form adducts with a family of tungsten(0) dinitrogen complexes (**37**$_W$), (**48**$_W$) and (**49**$_W$).[144] While equimolar mixtures of a tungsten complex with (**47**) have systematically led to mixtures of compounds, adding an excess of (**47**) (2-3 fold) has led to the formation of single compounds that had all in common the borylation of the terminal nitrogen of one of the N_2 ligands, the other being lost during the reaction. A remarkable ligand effect was noticed by the authors: with dinitrogen complexes (**37**$_W$) and (**48**$_W$), one equivalent of (**47**) dissociates a phosphine, and the vacant coordination sites are occupied by a dihydridobis(pentafluorophenyl)borate anion in compounds (**50**$_W$) and (**51**$_W$); however, with the depe-supported [depe = 1,2-bis(diethylphosphino)ethane] complex (**49**$_W$), no phosphine dissociation was observed upon treatment with 2 equivalent of (**47**) and complex (**52**$_W$) was obtained (Scheme 13).

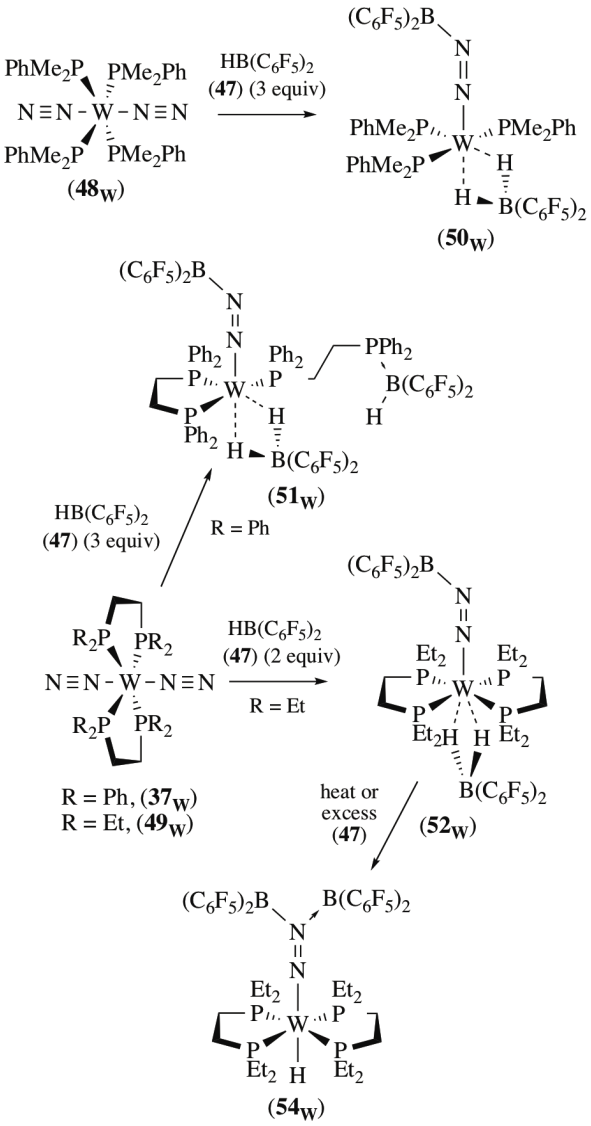

Scheme 13. Reactions of various W-N_2 complexes with $HB(C_6F_5)_2$ (**47**).

Monitoring of the reaction of (**49**$_W$) with one equivalent of (**47**) revealed a mixture of several compounds among which the adduct of (**49**$_W$) with (**47**) (**53**) could be partially characterized but not isolated. Notably, in IR spectroscopy, two previously unobserved bands were attributed to (**53**): a red-shifted $\nu(N_2)$ ($\Delta\nu(N_2)$ = –132 cm^{-1}) corresponding to the bridging N_2 (Figure 8). This remarkable shift reflects the high Lewis acidity of (**47**). A high energy $\nu(N_2)$ stretching frequency (2051 cm^{-1} in THF) was also observed, attesting that the other N_2 ligand was retained at this stage. In complexes (**50**$_W$)–(**52**$_W$), borylation of the N_2 ligand was proposed to operate through a similar mechanism than the one accounting for the formation of (**46**): B–H bond activation in (**53**) mediated by free (**47**) leads to the formation of the dihydridobis(pentafluorophenyl)borate anion and complexes (**50**$_W$)–(**52**$_W$). Notably, when (**52**$_W$) was heated or treated with a slight excess of (**47**), net hydride transfer was observed, leading to (**54**$_W$) (Scheme 13).

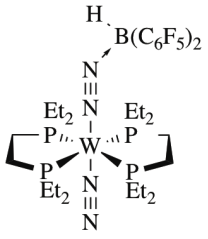

(**53**$_W$)

$\Delta\nu(N_2)$ –132 cm^{-1}

Figure 8. Adduct (**53**) observed during the reaction of (**47**) with (**49**$_W$).

4.3. Adducts of end-on dinitrogen iron complexes with strong main-group electrophiles: insights into catalysis

4.3.1. With boranes

As part of a study already mentioned above and aiming at testing the "push-pull hypothesis" concerning the mechanism of the nitrogenases,[13] Szymczak and his team have investigated the spectroscopic and electrochemical properties as well as electronic structures of Lewis pairs made of the end-on iron-dinitrogen complex [Fe(depe)$_2$(N$_2$)] (**1**) and various LAs.[61] To evaluate the generality of the observed augmented N_2 activation induced by s-block (section 2.2) and d-block (section 3.5) LAs complexation, a set of boranes BR_3 (R = 2,6-F_2Ph, 2,4,6-F_3Ph, C_6F_5, F, OC_6F_5) of variable Lewis acidities [quantified by the acceptor number (AN)[89]] were also reacted with (**1**). The [Fe(depe)$_2$(N$_2$-BR_3)] adducts (**55**)–(**59**) were obtained in quantitative yields and characterized by IR and NMR spectroscopy. The IR spectra revealed that the dinitrogen bond was considerably weakened as judged by the significant red-shift of the $\nu(N_2)$ stretching frequency, with $\Delta\nu(N_2)$ ranging from –101 to –172 cm^{-1}, tracking to the AN of the boranes (Table 4).

Table 4. Key parameters of the [Fe(depe)$_2$(N$_2$-BR_3)] adducts showing dependency to LAs' ANs.

[(depe)$_2$Fe(N$_2$BR$_3$)]	**AN of LA**	**$\Delta\nu(N_2)$ (cm^{-1})**	**E_{HOMO} (eV)**	**N_β charge (e$^-$)**	**$\pi^*(N_2)$ population (e$^-$)**	**E_{pa} (V) vs Fc^+/Fc**
(**1**) (no BR_3)	/	0	–3.73	–0.215	0.169	–1.72
R = 2,6-$C_6H_3F_2$, (**55**)	67.42	–101	–4.298	–0.252	0.217	–1.24
R = 2,4,6-$C_6H_2F_3$, (**56**)	69.07	–115	–4.38	–0.264	0.218	–1.05
R = C_6F_5, (**57**)	79.37	–143	–4.597	–0.296	0.222	–0.89
R = F, (**58**)	81.37	–146	–4.758	–0.377	0.220	n.c.
R = OC_6F_5, (**59**)	89.46	–172	–4.867	–0.369	0.228	–0.73

An X-ray structure was reported for the $B(C_6F_5)_3$ adduct (**57**), showing an elongated N–N bond (+0.04 Å) and a bent N-N-B arrangement. DFT calculations were performed in order to shed light on the electronic structure and bonding situation. Mixing of the vacant *p* orbital at boron and $\pi^*(N_2)$ is responsible for the dative N-B bonding, accounting for the bent geometry. Energetically, LA complexation leads to the stabilization of the HOMO of the complex, which is a combination of *d* orbitals and $\pi^*(N_2)$, giving it greater $\pi^*(N_2)$ character and therefore facilitating back-donation from the metal. The magnitude of stabilization and electron delocalization were found to track closely with the AN of the LAs. Counterintuitively, since LA coordination would be expected to quench the basicity of the terminal N (N_β), charges issued from NBO (Natural Bond Orbital) calculations were in line with increased negative charge. Several experimental facts came to support the computations:

i) in cyclic voltammetry, oxidation of the boron adducts occurred at more anodic potentials than (**1**) with differences consistent with the calculated stabilization energies.

ii) The ^{15}N isotopologue ^{15}N-(**57**) has a significantly shielded signal for the boron-bound nitrogen atom compared to the parent complex [N_β δ = –40.5 ppm for ^{15}N-(**1**); –119.8 ppm for ^{15}N-(**57**)]. This confirms the polarization of the dinitrogen moiety induced by LA complexation, electron density being localized on the terminal nitrogen atom.

iii) the increased negative charge on the terminal N makes it prone to react with electrophiles, reactions that are quite complicated with (**1**) owing to the occurrence of redox events. Treated with $HBAr^F_4$ (Ar^F = 3,5-$(F_3C)_2C_6H_3$), (**57**) underwent clean and selective protonation at N_β (Scheme 14).

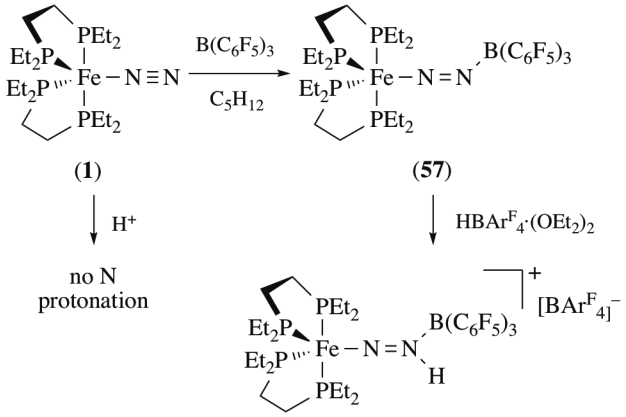

Scheme 14. Formation of adduct (**57**) and its selective protonation.

This body of work is remarkable in the way that the postulated influence of acidic residues within the active site of the nitrogenases on N_2 activation, that would be otherwise difficult to assess, has been verified using simple models. This illustrates well how synthetic N_2 complexes can help understand the functioning of the very complex nitrogenase enzymes. The same team has later reported push-pull activation of dinitrogen using H-bond donors.[62]

4.3.2. With Silicon cations

In biological as well as in homogeneous catalyses, characterization of intermediates is of primary importance to understand their mechanisms. In the previous section, characterization of a mono-protonated species by Geri *et al*. (Scheme 14) offers a snapshot of what may resemble elusive MN_2H intermediates formed after the first protonation step in catalytic N_2 reductions.[17,23] Facing difficulties to isolate such species, Ashley and coworkers cleverly made use of the more Lewis acidic Me_3Si^+ silylium ion as a proton mimic to characterize the first cationic silyldiazenido iron complexes.[149] Treatment of (**1**) or [$Fe(dmpe)_2(N_2)$] [(**60**), dmpe = 1,2-bis(dimethylphosphino)ethane] with $Me_3SiCl/KBAr^F_4$ afforded the ionic compounds (**61**) and (**62**) also bearing a bent N-N-Si arrangement (Scheme 15). IR data were in line with a notable weakening of the N–N bond. As expected with the strong LA Me_3Si^+, the $\nu(N_2)$ was dramatically shifted towards lower energies ($\Delta\nu(N_2)$ = –224 cm^{-1}). The X-ray diffraction structures of complexes (**61**) and (**62**) show an elongation of the N–N bond of *ca*. +0.05 Å, while the Fe–N bond displays greater double bond character than in (**1**) or (**60**). DFT calculations performed on the silyldiazenido complexes were in line with those run by Szymczak and co-workers regarding orbital interactions (*vide supra*). According to their diamagnetic character, trigonal bipyramid geometry and *d* orbital-centered HOMOs, the complexes were best described as Fe(0), d^8, rather than Fe(II), high spin d^6 species, although Mössbauer experiment were missing to support this proposition. This contrasts with the neutral silyldiazenido complexes prepared by the

reactions of silyl halides or pseudohalides with low valent iron N_2 complexes: in these cases, formal oxidation of the metal center was systematically observed.[81,150–153]

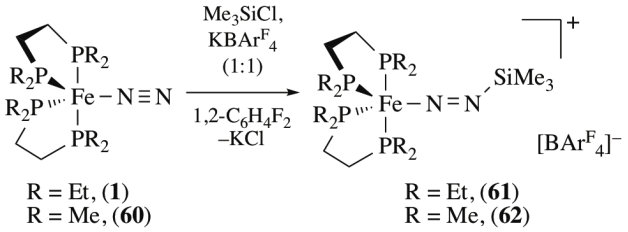

Scheme 15. Formal adducts of iron(0) dinitrogen complexes with silylium ions.

4.4. Adducts of p-block Lewis acids with end-on, side-on bimetallic dinitrogen complexes

4.4.1.Adducts with end-on, side-on dinitrogen tantalum complexes

In 2005, Fryzuk, Tuczek and coworkers jointly reported an in-depth study on the interaction of the tantalum end-on, side-on dinitrogen complex [{(NPN)Ta}$_2$(μ-H)$_2$(μ-η^1:η^2-N$_2$)] (**63**) ((NPN = (PhNSiMe$_2$CH$_2$)$_2$PPh), with various p-block LAs.[154] They had previously demonstrated by orbital analysis[155] a possible increased reactivity of the terminal nitrogen atom of (**63**) towards electrophiles and later showed that these reactions divided into two broad classes: addition reactions[156,157] or Lewis acid-base interactions. In order to better apprehend the reactivity of the N_2 ligand in (**63**), the interaction with group 13 LAs [GaMe$_3$, AlMe$_3$ and B(C$_6$F$_5$)$_3$] was explored. The 1:1 reaction of these LAs with (**63**) resulted in the immediate formation of the clean adducts [{(NPN)Ta}$_2$(μ-H)$_2$(μ-η^1:η^2-NNGaMe$_3$)] (**64**), [{(NPN)Ta}$_2$(μ-H)$_2$(μ-η^1:η^2-NNAlMe$_3$)] (**65**) and [{(NPN)Ta}$_2$(μ-H)$_2$(μ-η^1:η^2-NNB(C$_6$F$_5$)$_3$)] (**66**) (Scheme 16). By contrast, attempts to prepare adducts with BMe$_3$ and BEt$_3$ were unsuccessful.

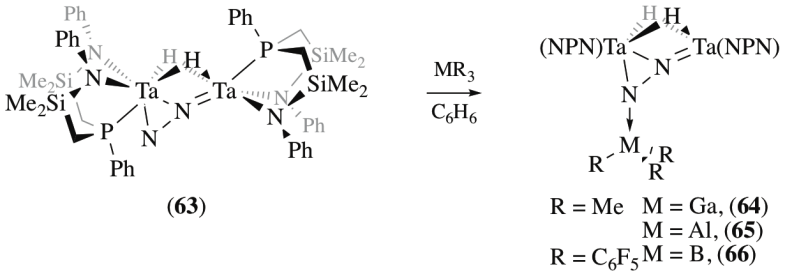

Scheme 16. Adducts of a side-on, end-on (NPN)Ta complex with GaMe$_3$, AlMe$_3$ and B(C$_6$F$_5$)$_3$.

The irreversibility of Lewis acid-base pairs formation was demonstrated by treating a solution of (**65**) with one equivalent of labelled [^{15}N]-(**63**), resulting in no reaction. Solid-state molecular structures of (**64**)–(**66**) were determined by X-ray crystallography. The Ta$_2$N$_2$ moiety show increased N–N distances ranging from 1.319(4) Å in the parent complex to 1.356(18), 1.363(7) and 1.393(7) Å in adducts (**64**)–(**66**), respectively. The level of N_2 activation correlates to the Lewis acidity of the group 13 electrophiles employed [quantified by the acceptor number (AN),[89] GaMe$_3$ < AlMe$_3$ (57.0) < B(C$_6$F$_5$)$_3$ (77.6)]. The M–N bond distances (M = Ga, Al or B) in (**64**)–(**66**) are 2.101(12), 1.993(5) and 1.584(9) Å, respectively. This observed shortening along the series is the result of decreasing covalent radii (R_{Ga} = 1.22(3) Å, R_{Al} = 1.21(4) Å, R_B = 0.84(3) Å) but also increasing Lewis acidity. These distances are in accordance with the formation of Lewis pairs, with B–N distances being in the range of the B–N bonds of tetracoordinated boron [average B–N bonds lengths in tetracoordinated boron species = 1.624 Å (SD = 0.0422 Å) gathered from 1161 structures of the SCD database]. ^{15}N NMR spectra of labelled [^{15}N]-

(**64**)–(**66**) exhibited two resonances; an upfield resonance corresponding to the shielded bridging N (N_α) and a downfield resonance assigned to the terminal N (N_β). The vibrational properties of (**64**)–(**66**) were measured by IR and resonance Raman spectroscopy (not shown) and found to be close to those of the parent complex (**63**), showing a slight decrease in the N–N stretching frequency in agreement with the observed elongation of the N–N bond (Table 5). The bonding situation in a model complex, $[\{PH_3(NH_2)_2Ta\}_2(\mu\text{-}H)_2(\mu\text{-}\eta^1\text{:}\eta^2\text{-}N_2\text{-}BH_3)]$, was investigated by means of DFT calculations. Dative bonding between boron and the terminal nitrogen occurs through mixing of a hybrid of the p_σ and a π bond of the N_2 fragment and the empty *p* orbital at boron. This leads to a decrease of the HOMO's energy, which corresponds to a bonding interaction of the metal centers' filled $d\pi$ orbitals with antibonding π^* of the dinitrogen ligand. Increased N_2 polarization can be traced according to Natural Charges (NCs) resulting from a Natural Population Analysis (NPA): the charge donation from the metal centers' filled d_π orbitals into the antibonding π^* orbitals of the dinitrogen ligand is increased, resulting in a net negative charge accumulation at the terminal N. Related to this work, the same team have explored the feasibility of a catalytic sequence to produce a functionalized hydrazine moiety (N_2B_4) from hydroboranes, N_2 and the Ta complex by examining the reaction of (**63**) with various hydroboranes.[157] No catalytic cycle could be completed but they discovered that with the hydroboranes 9-BBN, Cy_2BH and $H_2BCMe_2CHMe_2$, a new type of N–N bond cleavage proceeded subsequently to functionalization of the coordinated N_2 by B–H 1,2-addition over the Ta–N bond. Contrastingly, the reaction between (**63**) and the more Lewis acidic bis(pentafluorophenyl)borane (**47**) afforded the stable adduct (**67**) (not shown). Metric parameters collected by X-ray diffraction analysis as well as ^{15}N NMR data were close to those reported for the $B(C_6F_5)_3$ adduct (**66**).

Table 5. Selected metrical and spectroscopic parameters of complexes (**63**)–(**66**).

	63	**64**	**65**	**66**
d_{NN} (Å)	1.319(4)	1.356(18)	1.363(7)	1.393(7)
d_{MN} (Å)	n. a.	2.101(12)	1.993(5)	1.584(9)
^{15}N NMR (ppm)				
N_α	-20.4	-29.9	-33.1	-21.2
N_β	163.6	79.9	54.6	2.4
$\nu(N_2)$ (cm^{-1})	1165	1131	1132	1145

4.4.2.Adducts with end-on, side-on titanium dinitrogen complexes

The team of Hou has reported the synthesis of a new end-on, side-on dinitrogen dititanium hydride complex (**68**) that reacts with a variety of organometallic compounds such as $ZnMe_2$, $MgMe_2$, $AlMe_3$, $B(C_6F_5)_3$, PinBH and $PhSiH_3$.[158] Relevant to the present review is the reaction of complex (**68**) with one equivalent of $AlMe_3$ that leads to the formation of adduct (**69**) (Scheme 17). The ^{15}N NMR spectrum of the ^{15}N-labelled analogue [^{15}N]-(**69**) exhibits two resonances; an upfield resonance corresponding to the shielded bridging nitrogen nuclei (N_α: 46.6 ppm, slightly downfield shifted compared to [^{15}N]-(**68**): 43.2 ppm) and a downfield resonance assigned to the terminal N (N_β: 197.9 ppm, significantly upfield shifted compared to [^{15}N]-(**68**): 354.6 ppm). Solid-state molecular structure of (**69**) was determined by X-ray crystallography, which revealed an increase of the N-N distance from 1.296(3) Å in the parent complex (**68**) to 1.339(3) Å in (**69**), delineating the significant influence of LA coordination on the dinitrogen moiety. When a second equivalent of $AlMe_3$ was added and the reaction mixture heated at 60 °C, a new complex (**70**) containing a four-membered dialuminum dinitrido metallacycle was obtained. This structure was confirmed by an X-ray diffraction study and revealed shorter Al–N bond lengths than in adduct (**69**) [(**70**): 1.930(2) and 1.942(2) Å vs. (**69**): 1.982(2) Å]. The ^{15}N NMR spectrum of the [^{15}N]-labelled analogue of (**70**) shows one singlet at δ 194.5 ppm, suggesting that the two nitride

units are equivalent on the NMR time scale. The detection of possible intermediates of the reaction from (**69**) to (**70**) failed but the authors suggested that the addition of the second equivalent of $AlMe_3$ led to the formation of a dinitride/$AlMe_3$ adduct accompanied by H_2 loss and followed by Al–Me addition across the Ti=N unit.

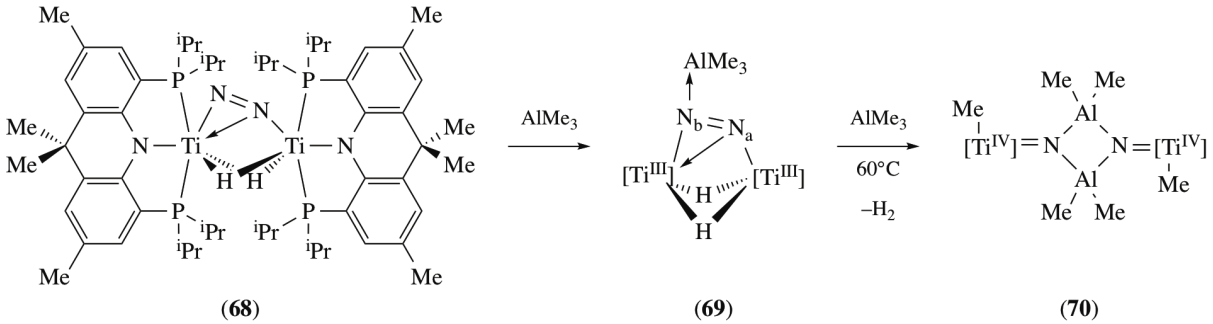

(**68**) (**69**) (**70**)

Scheme 17. Reaction of complex (**68**) with $AlMe_3$.

The reaction of $B(C_6F_5)_3$ with complex (**68**) was also performed and resulted in adduct (**71**) (Scheme 18). The ^{15}N NMR spectrum of the [^{15}N]-labelled analogue of (**71**) exhibited two doublets (N_α: 15.3 ppm and N_β: 93.9 ppm) shifted upfield compared to [^{15}N]-(**68**). Solid-state molecular structure of (**71**) was determined by X-ray crystallography and features an elongated N–N bond (1.343(3) Å) compared to (**68**); the B-N distance remained within the range of those observed in the case of tetracoordinated boron species ($d_{B\text{-}N\beta}$ = 1.578(4) Å), similarly to what was observed with the tantalum complex (**63**) (*vide supra*). When a diethyl ether solution of (**71**) was left at room temperature for 3 days, H_2 release was observed as well as a borylimido/μ_2-nitrido titanium complex (**72**), resulting from the splitting of the dinitrogen moiety and the migration of a C_6F_5 group from the boron to a titanium center. This body of work is a remarkable illustration of main-group LA coordination induced-N_2 splitting and that push-pull activation can trigger original reactivities for ligating dinitrogen.

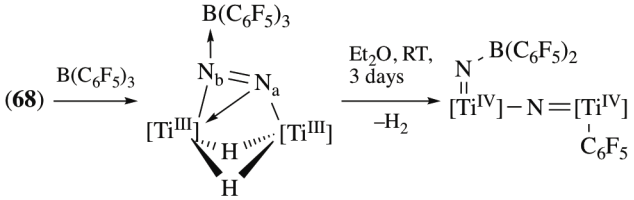

(**68**) (**71**) (**72**)

Scheme 18. Reaction of complex (**68**) with $B(C_6F_5)_3$.

5. P-BLOCK-ONLY SYSTEMS FOR PUSH-PULL ACTIVATION OF N_2

Although transition metals clearly dominate dinitrogen chemistry, the cost, scarcity, toxicity and environmental issues associated with them have pushed molecular chemists to find more sustainable alternative for N_2 activation. Argon matrix,[159–161] gas-phase[162] and in silico[163,164] studies have already demonstrated the ability of very reactive main group species to bind N_2. Recently, p-block metallomimetics, and borylenes in particular have emerged as effective N_2 fixation entities, while condensed and gas-phase models for FLP-type N_2 activation have also been proposed.

5.1. Borylenes for N_2 activation

In a remarkable article published in 2018, Braunschweig and co-workers have reported the first example of N_2 activation with a main group element, boron, in the condensed phase.[165,166] This was achieved thanks to the transient generation of a very reactive borylene species (**73**), in which a filled *p*

orbital and an orthogonal empty sp^2 orbital on the boron atom were proposed to play the role of the *d* orbitals of transition metals that are responsible for N_2 binding in dinitrogen complexes (Scheme 19). The solid-state structure of the N_2 activation product (**74**) reveals that two borylene moieties are implied with the dinitrogen molecule bridging them in a μ-η^1:η^1 fashion. The BNNB arrangement is bent with a B-N-N-B dihedral angle of ca. 110 °, which contrasts with bimetallic end-on bridging N_2 complexes that show a linear M-N-N-M motif. The N–N bond is in the range of double N–N bonds (1.248(4) Å).

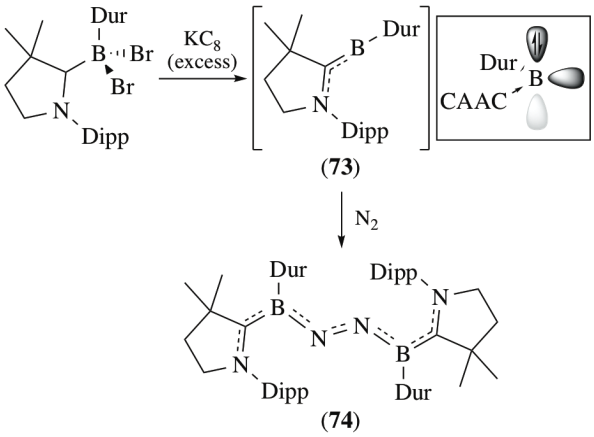

Scheme 19. Dinitrogen activation by borylene species (Dur = duryl, Dipp = 2,6-diisopropylphenyl, CAAC = cyclic alkyl amino carbene).

DFT calculations by the team of Mo with the use of block localized wavefunctions on a simplified model have shed light on this particular bonding.[167] They have shown that it is the result of two opposite and perpendicular push-pull channels and interactions with the orbitals of N_2 with π geometry only, as well as the uniqueness of borylenes for acting both as a Lewis acid and Lewis base. As with transition metals, N_2 activation in (**74**) is mainly the result of electron delocalization from the filled *p* orbital of the boron atoms into the π^* antibonding orbitals of the diatomic molecule. Pauli repulsion due to the filled *p* orbital on the boron atoms pushes the electrons populating the π/π^* orbitals of N_2 into the empty sp^2 orbital of the opposite borylene. This interaction differs from what is encountered in end-on, mono- and bi-metallic complexes of N_2 where the σ-type bonding occurs through N_2's lone pair overlap with the empty dz^2 of the metal (Scheme 20).

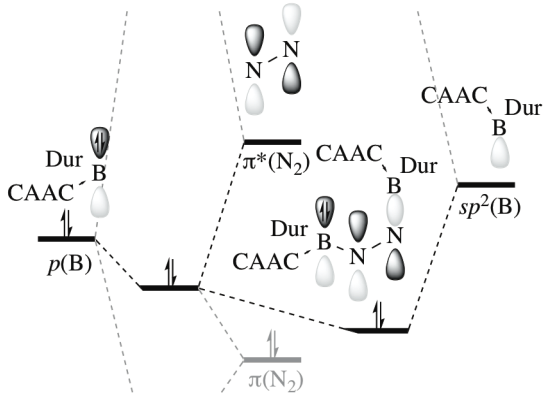

Scheme 20. Simplified molecular orbital showing one push-pull channel for N_2 activation in (**74**).

5.2. Boron-carbon FLP models for N_2 activation

5.2.1.In silico models: NHC-tethered borylenes

Zhu proposed in 2019 two theoretical examples of metal-free compounds that can activate dinitrogen with favorable thermodynamics and kinetics.[168] They examined the ability of intramolecular FLP consisting of either *sp*^{2}-hybridized, dicoordinated phosphorus, nitrogen or carbon as the Lewis basic site and *sp*-hybridized, dicoordinated boron as the Lewis acidic site. Thermodynamic calculations have shown that among the tested theoretical models, compounds (**75**) and (**76**) that both feature an N-heterocyclic carbene (NHC) can bind dinitrogen exergonically, thanks to the strength of the C–N bond formed in the N_2 activation products (**77**) and (**78**) as well as to their aromatic nature (Scheme 21).

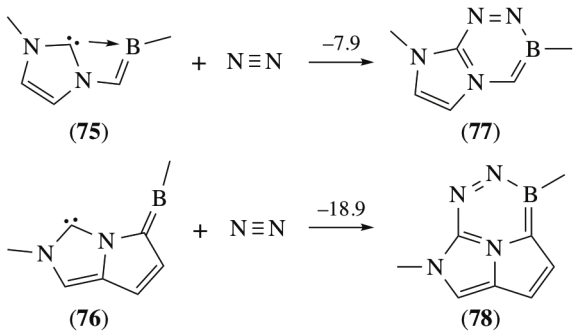

Scheme 21. Carbon-boron FLP systems for N_2 activation. ΔG given in kcal mol^{-1}.

The superiority of (**75**) over (**76**) for N_2 activation was established on both thermodynamic and kinetic grounds. First, after N_2 activation, greater delocalization of the π electrons gives greater aromaticity to (**78**) and therefore greater stabilization. This was highlighted by nucleus-independent chemical shift (NICS) calculations, as well as by the replacement of the *sp*-hybridized boron by an *sp*^{2}-hybridized one, resulting in significantly endergonic N_2 activation (ΔG = 40.8 kcal.mol^{-1}). Secondly, the significant donor-acceptor interaction between the boron atom and the carbene moiety in (**75**) imparts a kinetic disadvantage to the first elementary step of the transformation, which is the binding of N_2 to the *sp*-hybridized boron Lewis acid —the pull effect [activation barrier is 18.9 kcal.mol^{-1} for (**75**) and 8.3 kcal.mol^{-1} for (**76**)]. The Gibbs free energy of the second transition state of this transformation by which ring closure occurs through C–N bond formation is also reduced with enhanced aromaticity [11.3 kcal.mol^{-1} for (**75**) vs. 8.3 kcal.mol^{-1} for (**76**)].

5.2.2.Condensed phase models using diazo compounds

The team of Stephan recently published studies on diazo compounds that move the metal-free, FLP-type activation of dinitrogen a step closer to its realization.[169] Indeed, diazo compounds can be viewed as the products of N_2 binding over carbenes. In a previous report, they showed that diazomethanes liberate N_2 in the presence of boranes and insertion of the formally divalent carbon into a B–C bond was observed.[170] In 2017, they continued to explore the reactivity of diazomethane with strongly Lewis acidic boranes such as $HB(C_6F_5)_2$ (**47**) and $B(C_6F_5)_3$ (**41**).[171] The reaction of diphenyldiazomethane Ph_2CN_2 (**79**) with (**47**) resulted in the rapid formation of compound (**80**) (Scheme 22). It was identified by NMR spectra analysis as the product of 1,1-hydroboration of the terminal nitrogen atom by (**47**). The ^{1}H NMR displayed a peak at 8.77 ppm assignable to a single NH proton. An X-ray diffraction study revealed the double and single bond characters of the C–N and N–N linkages, respectively. DFT calculation showed that the reaction proceeds first by adduct formation between (**47**) and (**79**) followed by a 3-center, 2-electron-bond B-H-N transition state that allows the migration of the H atom from the boron to the proximal nitrogen. Two other synthetic pathways were found for the formation of (**80**) both implying the initial formation of an adduct between either (**47**) or (**41**) and benzophenone

hydrazone. Upon heating, these adducts released H_2 [with (**47**)] or HC_6F_5 [with (**41**)] leading to the formation of the covalent B–N bond in (**80**).

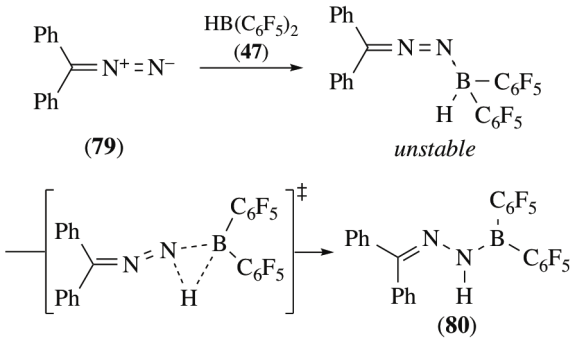

Scheme 22. 1,1-hydroboration of diphenyldiazomethane (**79**) by borane (**47**).

A thermally unstable adduct (**81**) could be isolated from the reaction between (**79**) and $B(C_6F_5)_3$ at –78 °C (Scheme 23). It was characterized by NMR spectroscopy analysis: upfield ^{11}B NMR shift and the reduced *meta-para* gap of the fluorine resonances compared to those of free $B(C_6F_5)_3$ were consistent with the formation of an adduct. IR data displayed absorption bands characteristic of C–N and N–N double bonds. Despite the sensitivity of (**81**), an X-ray diffraction study could be performed and confirmed the spectroscopic data (d_{CN} = 1.278(8) Å, d_{NN} = 1.177(7) Å, d_{BN} = 1.65(1) Å). Compared to the above-discussed "hybrid" metal boron templates (**44**) and (**57**) (sections 4.2 and 4.3.1)reported by the teams of Szymczak and Simonneau, the N–N bond length is shorter in (**81**), while the B–N linkage is significantly longer. The N-N-B arrangement is also bent, however, in (**81**) the N-N-B angle is much smaller [125 ° vs ca. 140 ° for (**44**) and (**57**)], most probably as the result of reduced steric repulsion between the boron and carbene substituents than with the phosphine ligands in (**44**) and (**57**). As the temperature is raised, (**81**) evolves dinitrogen. The authors have proposed, on the basis of partial characterization data, that the adduct of diphenylcarbene with (**41**), $Ph_2C(B(C_6F_5)_3)$, was formed (not shown).

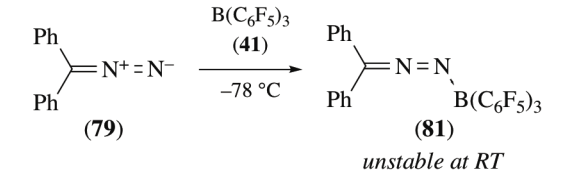

Scheme 23. Reaction of diphenyldiazomethane (**79**) with $B(C_6F_5)_3$ (**41**).

The successful isolation of (**81**) foreshadowed the possibility of FLP-N_2 chemistry. In a parallel study, the Stephan research group recently showed that weak Lewis acid-base adducts can be stabilized by one electron reduction promoted by decamethylferrocene, which afforded novel anions and a new strategy for small molecule activation.[172] They next explored the possibility of stabilizing the weak B···N interaction of diazomethane-borane adducts by single electron transfer (SET) (Scheme 24).[173] The adduct between diphenyldiazomethane (**79**) and $B(C_6F_5)_3$ (**41**) was reacted at –35 °C with one equivalent of decamethylcobaltocene to readily give two new compounds (**82**) and (**83**) containing a tetracoordinated boron atom according to ^{11}B NMR. The ^{1}H NMR spectrum also revealed the formation of an N–H bond and the presence of a CH_2 fragment. These compounds could be separated by fractional recrystallization and were characterized by X-ray diffraction. Compound (**82**) was identified as a salt where the anionic part is a hydrazide-borane adduct with a significantly shorter B–N bond compared to (**81**) (d_{BN} = 1.539(7) Å vs. 1.65(1) Å). The H atom on compound (**82**) originates from the abstraction of one hydrogen of a Cp* methyl group which led to formation of compound (**83**) where

the hydrogen abstracted is replaced by the $[B(C_6F_5)_3]^-$ group. The reaction proceeded first by the formation of the unstable adduct (**81**) which is then reduced by Cp^*_2Co to give the transient diazomethane-borane adduct radical anion $[Ph_2CN_2B(C_6F_5)_3]^{\bullet-}$ (**84**). This species is then able to abstract a hydrogen atom from the metallocene to form (**82**) and (**83**). Strong support to this mechanism was brought by the absence of reaction between (**79**) and the $[HB(C_6F_5)_3]^-$ anion that would form after C–H activation by the $[B(C_6F_5)_3]^{\bullet-}$ radical-anion. Although attempts to observe this transient radical adduct were unsuccessful, the reaction between the fluorenyl analogue of (**79**), Cp^*_2Fe and $Al(C_6F_5)_3$ afforded a long-lived N-based radical (not shown) that was characterized by EPR spectroscopy. When the weaker Lewis acid BPh_3 was used, adduct (**85**) could not be observed but addition of Cp^*_2Cr resulted in a color change. Fractional crystallization allowed for the isolation of two new compounds (**86**) and (**87**) (Scheme 24). While the latter is comparable to (**82**), in this case, the H atom carried by the terminal nitrogen originates from an intermolecular H atom transfer. Indeed, (**86**) results from an intramolecular cyclization of (**88**) that issues a 5-membered ring upon addition of the nitrogen radical to an *ortho* aromatic position. The delocalized aryl radical intermediate generated after the addition transfers an H atom to free (**79**) that eventually delivers (**87**) by reduction by Cp^*_2Cr and reaction with BPh_3.

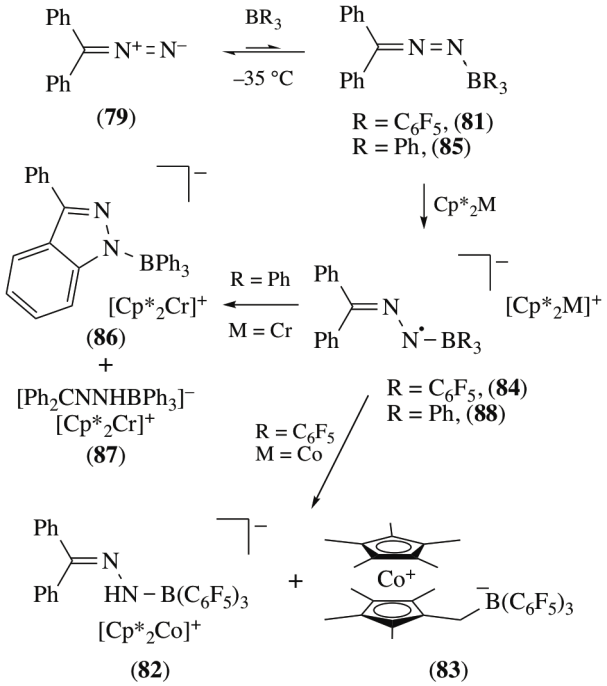

Scheme 24. Reactivity of diazomethanes-boranes adducts upon one electron reduction.

Although this body of work employs compounds not made from dinitrogen, they offer a view of what could be the reactivity of push-pull, FLP-type N_2 activation compounds. Especially, the one electron reduction of borane-diazomethanes adducts demonstrates that highly reactive N centered radicals can be generated using these systems.

6. CONCLUSIONS

We hope we have offered with the present article a concise but as exhaustive as possible view on the activation of N_2 through a push-pull mechanism. The population of N_2 antibonding orbitals, key to N_2 activation by an electron-rich element, can be greatly enhanced if a second, comparatively electron-poorer element, interacts concomitantly with the diatomic. Although the level of N_2 activation is significantly lower than those reached with homobimetallic systems using reducing metals, push-pull

activation is generally achieved through redox-neutral processes and grants dinitrogen a high level of polarization, which has, in some instances, allowed the discovery of original reactivities. With the emergence of strongly Lewis acidic compounds, we are confident that new systems will be examined that will permit to expand the scope of reactivities known for coordinated N_2.

7. ACKNOWLEDGEMENTS

A. S. and D. S. acknowledge the European Research Council for funding (grant agreement 757501). A. C. is grateful to the French Ministry of Superior Education and Research for a Ph. D. fellowship.

8. ABBREVIATIONS AND ACRONYMS

AN acceptor number

Ar^F 3,5-bis(trifluoromethyl)phenyl

BBN borabicyclononane

CAAC cyclic alkyl amino carbene

depe 1,2-bis(diethylphosphino)ethane

Dipp 2,6-diisopropylphenyl

dmpe 1,2-bis(dimethylphosphino)ethane

dppe 1,2-bis(diphenylphosphino)ethane

Dur duryl,

FLP frustrated Lewis pair

LA Lewis acid

NC Natural Charges

NMR Nuclear magnetic resonance

NPA Natural Population Analysis

OEP octaethylporphyrinate

SET single electron transfer

TM transition metal

TMS trimethylsilyl

TTP tetra(*p*-tolyl)porphyrinate

9. REFERENCES

1. A. D. Allen and C. V Senoff, *Chem. Commun.*, 1965, 621–622.

2. *Transition Metal-Dinitrogen Complexes: Preparation and Reactivity*, ed. Y. Nishibayashi, Wiley-VCH Verlag GmbH & Co. KGaA, Weinheim, 2019.

3. R. J. Burford and M. D. Fryzuk, *Nat. Rev. Chem.*, 2017, **1**, 26.

4. M. D. Walter, *Recent Advances in Transition Metal-Catalyzed Dinitrogen Activation*, in *Advances in Organometallic Chemistry*, ed. P. J. Pérez, Academic Press, 2016, vol. 65, pp. 261–377.

5. C. Köthe and C. Limberg, *Z. Anorg. Allg. Chemie*, 2015, **641**, 18–30.

6. N. Khoenkhoen, B. de Bruin, J. N. H. Reek and W. I. Dzik, *Eur. J. Inorg. Chem.*, 2015, **2015**, 567–598.

7. M. D. Fryzuk, *Chem. Commun.*, 2013, **49**, 4866–4868.

8. J. Ballmann, R. F. Munha and M. D. Fryzuk, *Chem. Commun.*, 2010, **46**, 1013–1025.

9. S. Gambarotta and J. Scott, *Angew. Chem. Int. Ed.*, 2004, **43**, 5298–5308.

10. B. A. MacKay and M. D. Fryzuk, *Chem. Rev.*, 2004, **104**, 385–402.

11. M. Rohde, D. Sippel, C. Trncik, S. L. A. Andrade and O. Einsle, *Biochemistry*, 2018, **57**, 5497–5504.

12. Y. Hu and M. W. Ribbe, *Angew. Chem. Int. Ed.*, 2016, **55**, 8216–8226.

13. B. M. Hoffman, D. Lukoyanov, Z.-Y. Yang, D. R. Dean and L. C. Seefeldt, *Chem. Rev.*, 2014, **114**, 4041–4062.

14. B. M. Hoffman, D. Lukoyanov, D. R. Dean and L. C. Seefeldt, *Acc. Chem. Res.*, 2013, **46**, 587–595.

15. B. M. Hoffman, D. R. Dean and L. C. Seefeldt, *Acc. Chem. Res.*, 2009, **42**, 609–619.

16. J. B. Howard and D. C. Rees, *Proc. Natl. Acad. Sci.*, 2006, **103**, 17088–17093.

17. M. A. Nesbit, P. H. Oyala and J. C. Peters, *J. Am. Chem. Soc.*, 2019, **141**, 8116–8127.

18. M. Tamizmani and C. Sivasankar, *Eur. J. Inorg. Chem.*, 2017, **2017**, 4239–4245.

19. M. T. Mock, A. W. Pierpont, J. D. Egbert, M. O'Hagan, S. Chen, R. M. Bullock, W. G. Dougherty, W. S. Kassel and R. Rousseau, *Inorg. Chem.*, 2015, **54**, 4827–4839.

20. Y. Ohki, K. Aoyagi and H. Seino, *Organometallics*, 2015, **34**, 3414–3420.

21. J. S. Anderson, G. E. Cutsail, J. Rittle, B. A. Connor, W. A. Gunderson, L. Zhang, B. M. Hoffman and J. C. Peters, *J. Am. Chem. Soc.*, 2015, **137**, 7803–7809.

22. J. Rittle and J. C. Peters, *J. Am. Chem. Soc.*, 2016, **138**, 4243–4248.

23. D. V. Yandulov and R. R. Schrock, *Inorg. Chem.*, 2005, **44**, 1103–1117.

24. G. J. Leigh, *Acc. Chem. Res.*, 1992, **25**, 177–181.

25. M. Jimenez-Tenorio, M. C. Puerta, P. Valerga and D. L. Hughes, *J. Chem. Soc. Dalt. Trans.*, 1994, 2431–2436.

26. Y. Nishibayashi, S. Iwai and M. Hidai, *Science*, 1998, **279**, 540–542.

27. Y. Nishibayashi, I. Wakiji, K. Hirata, M. R. DuBois and M. Hidai, *Inorg. Chem.*, 2001, **40**, 578–580.

28. J. Chatt, R. L. Richards, J. R. Sanders and J. E. Fergusson, *Nature*, 1969, **221**, 551–552.

29. J. Chatt, G. A. Heath and R. L. Richards, *J. Chem. Soc. Chem. Commun.*, 1972, 1010–1011.

30. J. Chatt, G. A. Heath and R. L. Richards, *J. Chem. Soc. Dalt. Trans.*, 1974, 2074–2082.

31. G. A. Heath, R. Mason and K. M. Thomas, *J. Am. Chem. Soc.*, 1974, **96**, 259–260.

32. J. Chatt, A. J. Pearman and R. L. Richards, *Nature*, 1975, **253**, 39–40.

33. M. Hidai, T. Kodama, M. Sato, M. Harakawa and Y. Uchida, *Inorg. Chem.*, 1976, **15**, 2694–2697.

34. J. Chatt, A. J. Pearman and R. L. Richards, *J. Chem. Soc. Dalt. Trans.*, 1977, 2139–2142.

35. J. Chatt, A. J. Pearman and R. L. Richards, *J. Chem. Soc. Dalt. Trans.*, 1977, 1852–1860.

36. M. Hidai, Y. Mizobe, T. Takahashi and Y. Uchida, *Chem. Lett.*, 1978, **7**, 1187–1188.

37. T. Takahashi, Y. Mizobe, M. Sato, Y. Uchida and M. Hidai, *J. Am. Chem. Soc.*, 1979, **101**, 3405–3407.

38. T. Takahashi, Y. Mizobe, M. Sato, Y. Uchida and M. Hidai, *J. Am. Chem. Soc.*, 1980, **102**, 7461–7467.

39. A. Yamamoto, Y. Miura, T. Ito, H. L. Chen, K. Iri, F. Ozawa, K. Miki, T. Sei, N. Tanaka and N. Kasai, *Organometallics*, 1983, **2**, 1429–1436.

40. S. L. Foster, S. I. P. Bakovic, R. D. Duda, S. Maheshwari, R. D. Milton, S. D. Minteer, M. J. Janik, J. N. Renner and L. F. Greenlee, *Nat. Catal.*, 2018, **1**, 490–500.

41. N. Stucke, B. M. Flöser, T. Weyrich and F. Tuczek, *Eur. J. Inorg. Chem.*, 2018, **2018**, 1337–1355.

42. *Nitrogen Fixation*, ed. Y. Nishibayashi, Springer International Publishing AG, Cham, Switzerland, 2017.

43. Y. Roux, C. Duboc and M. Gennari, *ChemPhysChem*, 2017, **18**, 2606–2617.

44. Y. Tanabe and Y. Nishibayashi, *Chem. Rec.*, 2016, **16**, 1549–1577.

45. H.-P. Jia and E. A. Quadrelli, *Chem. Soc. Rev.*, 2014, **43**, 547–564.

46. K. C. MacLeod and P. L. Holland, *Nat. Chem.*, 2013, **5**, 559–565.

47. J. W. Erisman, M. A. Sutton, J. Galloway, Z. Klimont and W. Winiwarter, *Nat. Geosci.*, 2008, **1**, 636.

48. G. Ertl, *Angew. Chem. Int. Ed.*, 2008, **47**, 3524–3535.

49. M. Appl, *Ullmann's Encycl. Ind. Chem.*, 2006.

50. R. Schlögl, *Angew. Chem. Int. Ed.*, 2003, **42**, 2004–2008.

51. V. Smil, *Enriching the Earth: Fritz Haber, Carl Bosch, and the Transformation of World Food Production*, Mit Press, 2001.

52. V. Smil, *Nature*, 1999, **400**, 415.

53. J. R. Jennings, *Catalytic Ammonia Synthesis: Fundamentals and Practice*, Springer, 1991.

54. J. Chatt, J. R. Dilworth, H. P. Gunz, G. J. Leigh and J. R. Sanders, *J. Chem. Soc. D Chem. Commun.*, 1970, 90–91.

55. J. Chatt, J. R. Dilworth, G. J. Leigh and R. L. Richards, *J. Chem. Soc. D Chem. Commun.*, 1970, 955–956.

56. J. Chatt, R. C. Fay and R. L. Richards, *J. Chem. Soc. A Inorganic, Phys. Theor.*, 1971, 702–704.

57. J. Chatt, R. H. Crabtree and R. L. Richards, *J. Chem. Soc. Chem. Commun.*, 1972, 534.

58. J. Chatt, R. H. Crabtree, E. A. Jeffery and R. L. Richards, *J. Chem. Soc. Dalt. Trans.*, 1973, 1167–

1172.

59. H. Kristen, *Wissenschaftliche Zeitschrift der Univ. Rostock, Math. R.*, 1976, **25**, 1123–1130.

60. D. Lloyd and H. McNab, *Angew. Chem. Int. Ed. Engl.*, 1976, **15**, 459–468.

61. J. B. Geri, J. P. Shanahan and N. K. Szymczak, *J. Am. Chem. Soc.*, 2017, **139**, 5952–5956.

62. J. P. Shanahan and N. K. Szymczak, *J. Am. Chem. Soc.*, 2019, **141**, 8550–8556.

63. A. Simonneau and M. Etienne, *Chem. Eur. J.*, 2018, **24**, 12458–12463.

64. A. J. Ruddy, D. M. C. Ould, P. D. Newman and R. L. Melen, *Dalton Trans.*, 2018, **47**, 10377–10381.

65. A. Mittasch, *Geschichte der Ammoniaksynthese*, Verlag Chemie, 1951.

66. M. T. Rodgers and P. B. Armentrout, *Chem. Rev.*, 2016, **116**, 5642–5687.

67. D. J. Cram, *Science*, 1988, **240**, 760–767.

68. M. Shibasaki, H. Sasai and T. Arai, *Angew. Chem. Int. Ed. Engl.*, 1997, **36**, 1236–1256.

69. T. Chantarojsiri, J. W. Ziller and J. Y. Yang, *Chem. Sci.*, 2018, **9**, 2567–2574.

70. M. Sai and S. Matsubara, *Synlett*, 2014, **25**, 2067–2071.

71. J. L. Crossland and D. R. Tyler, *Coord. Chem. Rev.*, 2010, **254**, 1883–1894.

72. N. Hazari, *Chem. Soc. Rev.*, 2010, **39**, 4044–4056.

73. R. H. Holm, P. Kennepohl and E. I. Solomon, *Chem. Rev.*, 1996, **96**, 2239–2314.

74. E. I. Solomon, R. K. Szilagyi, S. DeBeer George and L. Basumallick, *Chem. Rev.*, 2004, **104**, 419–458.

75. A. S. Borovik, *Acc. Chem. Res.*, 2005, **38**, 54–61.

76. H. M. Neu, R. A. Baglia and D. P. Goldberg, *Acc. Chem. Res.*, 2015, **48**, 2754–2764.

77. M. D. Toney, E. Hohenester, S. W. Cowan and J. N. Jansonius, *Science*, 1993, **261**, 756–759.

78. X. Zhou, S. Kay and M. D. Toney, *Biochemistry*, 1998, **37**, 5761–5769.

79. J.-P. F. Cherry, F. H. Stephens, M. J. A. Johnson, P. L. Diaconescu and C. C. Cummins, *Inorg. Chem.*, 2001, **40**, 6860–6862.

80. D. V. Yandulov and R. R. Schrock, *Science*, 2003, **301**, 76–78.

81. G. Ung and J. C. Peters, *Angew. Chem. Int. Ed.*, 2015, **54**, 532–535.

82. G. P. Connor and P. L. Holland, *Catal. Today*, 2017, **286**, 21–40.

83. M. B. O'Donoghue, N. C. Zanetti, W. M. Davis and R. R. Schrock, *J. Am. Chem. Soc.*, 1997, **119**, 2753–2754.

84. M. B. O'Donoghue, W. M. Davis, R. R. Schrock and W. M. Reiff, *Inorg. Chem.*, 1999, **38**, 243–252.

85. G. E. Greco and R. R. Schrock, *Inorg. Chem.*, 2001, **40**, 3861–3878.

86. T. A. Betley and J. C. Peters, *J. Am. Chem. Soc.*, 2004, **126**, 6252–6254.

87. T. R. Dugan, K. C. MacLeod, W. W. Brennessel and P. L. Holland, *Eur. J. Inorg. Chem.*, 2013, **2013**,

3891–3897.

88. S. L. Apps, P. W. Miller and N. J. Long, *Chem. Commun.*, 2019, **55**, 6579–6582.

89. M. A. Beckett, G. C. Strickland, J. R. Holland and K. S. Varma, *Polymer*, 1996, **37**, 4629–4631.

90. L. G. Pap, A. Couldridge, N. Arulsamy and E. Hulley, *Dalton Trans.*, 2019, **48**, 11004–11017.

91. J. W. Steed, *Coord. Chem. Rev.*, 2001, **215**, 171–221.

92. D. F. Harrison, E. Weissberger and H. Taube, *Science*, 1968, **159**, 320–322.

93. M. D. Fryzuk and S. A. Johnson, *Coord. Chem. Rev.*, 2000, **200**–**202**, 379–409.

94. M. D. Fryzuk, J. B. Love, S. J. Rettig and V. G. Young, *Science*, 1997, **275**, 1445–1447.

95. J. A. Pool, E. Lobkovsky and P. J. Chirik, *Nature*, 2004, **427**, 527–530.

96. D. J. Knobloch, E. Lobkovsky and P. J. Chirik, *Nat. Chem.*, 2010, **2**, 30–35.

97. J. Ballmann, A. Yeo, B. O. Patrick and M. D. Fryzuk, *Angew. Chem. Int. Ed.*, 2011, **50**, 507–510.

98. S. P. Semproni, G. W. Margulieux and P. J. Chirik, *Organometallics*, 2012, **31**, 6278–6287.

99. D. J. Knobloch, S. P. Semproni, E. Lobkovsky and P. J. Chirik, *J. Am. Chem. Soc.*, 2012, **134**, 3377–3386.

100. S. P. Semproni and P. J. Chirik, *J. Am. Chem. Soc.*, 2013, **135**, 11373–11383.

101. C. E. Laplaza and C. C. Cummins, *Science*, 1995, **268**, 861–863.

102. I. Klopsch, E. Y. Yuzik-Klimova and S. Schneider, *Top. Organomet. Chem.*, 2017, **60**, 71–112.

103. A. L. Odom, P. L. Arnold and C. C. Cummins, *J. Am. Chem. Soc.*, 1998, **120**, 5836–5837.

104. D. J. Mindiola, K. Meyer, J.-P. F. Cherry, T. A. Baker and C. C. Cummins, *Organometallics*, 2000, **19**, 1622–1624.

105. T. Takahashi, T. Kodama, A. Watakabe, Y. Uchida and M. Hidai, *J. Am. Chem. Soc.*, 1983, **105**, 1680–1682.

106. Y. Mizobe, Y. Yokobayashi, H. Oshita, T. Takahashi and M. Hidai, *Organometallics*, 1994, **13**, 3764–3766.

107. J. Chatt, J. R. Dilworth and G. J. Leigh, *J. Chem. Soc. D Chem. Commun.*, 1969, 687–688.

108. J. Chatt, J. R. Dilworth, R. L. Richards and J. R. Sanders, *Nature*, 1969, **224**, 1201–1202.

109. J. A. Ibers and B. R. Davis, *Inorg. Chem.*, 1971, **10**, 578–585.

110. M. Mercer, R. H. Crabtree and R. L. Richards, *J. Chem. Soc. Chem. Commun.*, 1973, 808–809.

111. M. Mercer, *J. Chem. Soc. Dalt. Trans.*, 1974, 1637–1640.

112. P. L. Holland, *Dalton Trans.*, 2010, **39**, 5415–5425.

113. P. D. Cradwick, J. Chatt, R. H. Crabtree and R. L. Richards, *J. Chem. Soc. Chem. Commun.*, 1975, 351–352.

114. P. D. Cradwick, *J. Chem. Soc. Dalt. Trans.*, 1976, 1934–1936.

115. J. Chatt and R. L. Richards, *J. Less Common Met.*, 1977, **54**, 477–484.

116. R. Robson, *Inorg. Chem.*, 1974, **13**, 475–479.

117. P. M. Hamilton, R. McBeth, W. Bekebrede and H. H. Sisler, *J. Am. Chem. Soc.*, 1953, **75**, 2881–2883.

118. S. Donovan-Mtunzi, R. L. Richards and J. Mason, *J. Chem. Soc. Dalt. Trans.*, 1984, 2429–2433.

119. S. Donovan-Mtunzi, R. L. Richards and J. Mason, *J. Chem. Soc. Dalt. Trans.*, 1984, 469–474.

120. J. P. Collman, J. E. Hutchison, M. A. Lopez and R. Guilard, *J. Am. Chem. Soc.*, 1992, **114**, 8066–8073.

121. J. P. Collman, J. E. Hutchison, M. S. Ennis, M. A. Lopez and R. Guilard, *J. Am. Chem. Soc.*, 1992, **114**, 8074–8080.

122. Q.-F. Zhang, J. L. C. Chim, W. Lai, W.-T. Wong and W.-H. Leung, *Inorg. Chem.*, 2001, **40**, 2470–2471.

123. C. A. Reed and F. Guiset, *J. Am. Chem. Soc.*, 1996, **118**, 3281–3282.

124. S. B. Seymore and S. N. Brown, *Inorg. Chem.*, 2002, **41**, 462–469.

125. S. B. Seymore and S. N. Brown, *Inorg. Chem.*, 2006, **45**, 9540–9550.

126. A. D. Piascik and A. E. Ashley, *Group 8 Transition Metal–Dinitrogen Complexes*, in *Transition Metal-Dinitrogen Complexes: Preparation and Reactivity*, ed. Y. Nishibayashi, Wiley-VCH Verlag GmbH & Co. KGaA, Weinheim, Germany, 2019, pp. 285–335.

127. N. Mézailles, *Group 6 Transition Metal–Dinitrogen Complexes*, in *Transition Metal-Dinitrogen Complexes: Preparation and Reactivity*, ed. Y. Nishibayashi, Weinheim, Germany, 2019, pp. 221–269.

128. M. L. H. Green and W. E. Silverthorn, *J. Chem. Soc. Dalt. Trans.*, 1973, 301–306.

129. W. E. Silverthorn, *J. Chem. Soc. D Chem. Commun.*, 1971, 1310–1311.

130. L. D. Field, R. W. Guest and P. Turner, *Inorg. Chem.*, 2010, **49**, 9086–9093.

131. L. R. Doyle, P. J. Hill, G. G. Wildgoose and A. E. Ashley, *Dalton Trans.*, 2016, **45**, 7550–7554.

132. H. Broda, S. Hinrichsen, J. Krahmer, C. Nather and F. Tuczek, *Dalton Trans.*, 2014, **43**, 2007–2012.

133. J. Paradies, *Coord. Chem. Rev.*, 2019, **380**, 170–183.

134. D. W. Stephan, *Science*, 2016, **354**, http://science.sciencemag.org/content/354/6317/aaf7229.abstract.

135. D. W. Stephan and G. Erker, *Angew. Chem. Int. Ed.*, 2015, **54**, 6400–6441.

136. D. W. Stephan and G. Erker, *Angew. Chem. Int. Ed.*, 2010, **49**, 46–76.

137. G. C. Welch, R. R. S. Juan, J. D. Masuda and D. W. Stephan, *Science*, 2006, **314**, 1124–1126.

138. J. Lam, K. M. Szkop, E. Mosaferi and D. W. Stephan, *Chem. Soc. Rev.*, 2019, **48**, 3592–3612.

139. D. J. Scott, M. J. Fuchter and A. E. Ashley, *Chem. Soc. Rev.*, 2017, **46**, 5689–5700.

140. J. Paradies, *Angew. Chem. Int. Ed.*, 2014, **53**, 3552–3557.

141. V. Sumerin, K. Chernichenko, F. Schulz, M. Leskelä, B. Rieger and T. Repo, *Top. Curr. Chem.*, 2013, **332**, 111–155.

142. D. W. Stephan and G. Erker, in *Frustrated Lewis Pairs I: Uncovering and Understanding*, eds. G. Erker and D. W. Stephan, Springer Berlin Heidelberg, Berlin, Heidelberg, 2013, pp. 85–110.

143. M. Sajid, G. Kehr, C. G. Daniliuc and G. Erker, *Angew. Chem. Int. Ed.*, 2014, **53**, 1118–1121.

144. A. Simonneau, R. Turrel, L. Vendier and M. Etienne, *Angew. Chem. Int. Ed.*, 2017, **56**, 12268–12272.

145. S. Rendler and M. Oestreich, *Angew. Chem. Int. Ed.*, 2008, **47**, 5997–6000.

146. W. Nie, H. F. T. Klare, M. Oestreich, R. Fröhlich, G. Kehr and G. Erker, *Z. Naturforsch. B*, 2012, **67**, 987–994.

147. A. Y. Houghton, J. Hurmalainen, A. Mansikkamäki, W. E. Piers and H. M. Tuononen, *Nat. Chem.*, 2014, **6**, 983–988.

148. E. A. Patrick and W. E. Piers, *Chem. Commun.*, 2020, **56**, 841–853.

149. A. D. Piascik, P. J. Hill, A. D. Crawford, L. R. Doyle, J. C. Green and A. E. Ashley, *Chem. Commun.*, 2017, **53**, 7657–7660.

150. T. A. Betley and J. C. Peters, *J. Am. Chem. Soc.*, 2003, **125**, 10782–10783.

151. Y. Lee, N. P. Mankad and J. C. Peters, *Nat. Chem.*, 2010, **2**, 558–565.

152. P. A. Rudd, N. Planas, E. Bill, L. Gagliardi and C. C. Lu, *Eur. J. Inorg. Chem.*, 2013, **2013**, 3898–3906.

153. S. F. McWilliams, E. Bill, G. Lukat-Rodgers, K. R. Rodgers, B. Q. Mercado and P. L. Holland, *J. Am. Chem. Soc.*, 2018, **140**, 8586–8598.

154. F. Studt, B. A. MacKay, S. A. Johnson, B. O. Patrick, M. D. Fryzuk and F. Tuczek, *Chem. Eur. J.*, 2005, **11**, 604–618.

155. F. Studt, B. A. MacKay, M. D. Fryzuk and F. Tuczek, *J. Am. Chem. Soc.*, 2004, **126**, 280–290.

156. M. D. Fryzuk, B. A. MacKay, S. A. Johnson and B. O. Patrick, *Angew. Chem. Int. Ed.*, 2002, **41**, 3709–3712.

157. B. A. MacKay, S. A. Johnson, B. O. Patrick and M. D. Fryzuk, *Can. J. Chem.*, 2005, **83**, 315–323.

158. Z. Mo, T. Shima and Z. Hou, *Angew. Chem. Int. Ed.*, 2020, **59**, DOI:10.1002/anie.201916171.

159. G. Maier, H. P. Reisenauer, J. Henkelmann and C. Kliche, *Angew. Chem.*, 1988, **100**, 303.

160. M. Winkler and W. Sander, *J. Org. Chem.*, 2006, **71**, 6357–6367.

161. K. Edel, M. Krieg, D. Grote and H. F. Bettinger, *J. Am. Chem. Soc.*, 2017, **139**, 15151–15159.

162. J. Jin, G. Wang, M. Zhou, D. M. Andrada, M. Hermann and G. Frenking, *Angew. Chem. Int. Ed.*, 2016, **55**, 2078–2082.

163. M. M. Montero-Campillo, I. Alkorta and J. Elguero, *Sci. Rep.*, 2017, **7**, 6115.

164. A. M. Rouf, C. Dai, F. Xu and J. Zhu, *Adv. Theory Simulations*, 2020, **3**, 1900205.

165. D. L. J. Broere and P. L. Holland, *Science*, 2018, **359**, 871–871.

166. M.-A. Légaré, G. Bélanger-Chabot, R. D. Dewhurst, E. Welz, I. Krummenacher, B. Engels and H. Braunschweig, *Science*, 2018, **359**, 896–900.

167. H. Zhang, R. Yuan, W. Wu and Y. Mo, *Chem. Eur. J.*, 2020, **26**, 2619–2625.

168. J. Zhu, *Chem. Asian J.*, 2019, **14**, 1413–1417.

169. R. L. Melen, *Angew. Chem. Int. Ed.*, 2018, **57**, 880–882.

170. R. C. Neu, C. Jiang and D. W. Stephan, *Dalton Trans.*, 2013, **42**, 726–736.

171. C. Tang, Q. Liang, A. R. Jupp, T. C. Johnstone, R. C. Neu, D. Song, S. Grimme and D. W. Stephan, *Angew. Chem. Int. Ed.*, 2017, **56**, 16588–16592.

172. L. L. Liu, L. L. Cao, Y. Shao and D. W. Stephan, *J. Am. Chem. Soc.*, 2017, **139**, 10062–10071.

173. L. L. Cao, J. Zhou, Z.-W. Qu and D. W. Stephan, *Angew. Chem. Int. Ed.*, 2019, **58**, 18487–18491.